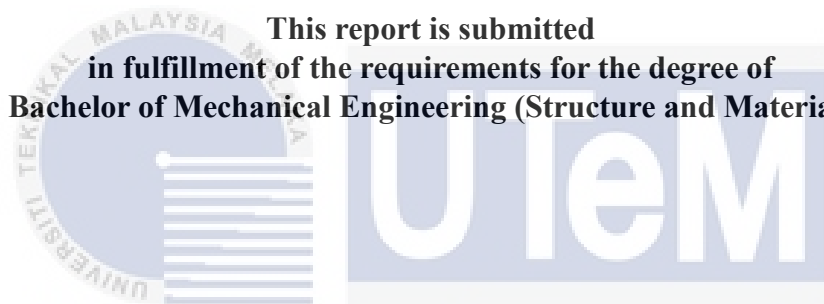


THE SAW DUST FILLED TUBE UNDER AXIAL LOADING

ONG XIONG HUI

**This report is submitted
in fulfillment of the requirements for the degree of
Bachelor of Mechanical Engineering (Structure and Material)**



اونيورسيتي تيكنيكل مليسيا ملاك

UNIVERSITI TEKNIKAL MALAYSIA MELAKA
Faculty of Mechanical Engineering

UNIVERSITI TEKNIKAL MALAYSIA MELAKA

2017

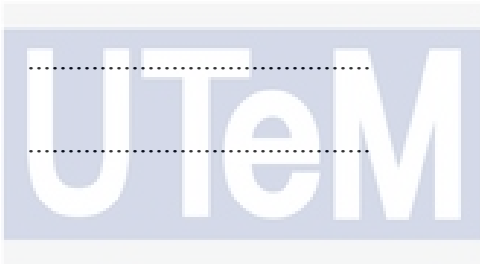
DECLARATION

I declare that this project report entitled “The Saw Dust Filled Tube under Axial Loading”
is the result of my own work except as cited in the references

Signature :

Name :

Date :



اونيورسيتي تيكنيكل مليسيا ملاك
UNIVERSITI TEKNIKAL MALAYSIA MELAKA

APPROVAL

I hereby declare that I have read this project report and in my opinion this report is sufficient in terms of scope and quality for the award of the degree of Bachelor of Mechanical Engineering (Structure & Materials).



Signature :

Name of Supervisor :

Date :

اونيورسيتي تيكنيكل مليسيا ملاك

UNIVERSITI TEKNIKAL MALAYSIA MELAKA

DEDICATION

To my beloved mother and father



ABSTRACT

Impact energy absorption device is one of the essential structural components used in safety application. It performs its services by reducing and absorbing the excessive kinetic energy to protect users from injury. Due to this safety purpose, impact energy absorption device is explored. Occasionally, metallic tubes are mostly used as the impact energy absorbing elements. Aluminium tube, as one type of the metallic tube is investigated and analyzed in this project. A development idea is laid out by introducing saw dust as filled material into the impact energy absorption device. This project was carried out to study the effect of saw dust on the collapse behavior and energy absorption performance to enhance the energy absorption device. Three different types of aluminium tubes were used, one circular and two different sizes of square aluminium tubes are filled with saw dust at different density and compressed axially by quasi-static loading. This project started with reviewing the previous researches to understand the theories and information which related to the present study. It was found that the material properties, mechanical properties and size of the tube greatly affect the deformation behavior and energy absorption performance. Following with this, tensile test and axial compression test experiments have been conducted in this project. Tensile test was carried out to investigate and determine the mechanical properties of aluminium tube. From the tensile test result obtained, the mechanical properties were later used to evaluate the theoretical mean load. While axial compression experiment involved the density setup for tube filled with saw dust and the observation of tube deformation pattern. Both hollow and saw dust filled aluminium tubes were compressed by INSTRON testing machine to obtain the load displacement characteristics. From load displacement curve, the densification point, plastic wavelength, mean load, energy absorption, and specific energy were determined and analyzed. Theoretical calculation for mean load, plastic wavelength and energy absorbed were also evaluated as well and compared with the experimental result. Both results show that the presence of saw dust affects the mean crushing load and energy absorption.

ABSTRAK

Peranti penerapan daya hentaman merupakan satu komponen struktur yang penting digunakan dalam aplikasi keselamatan. Peranti ini melaksanakan perkhidmatannya dengan cara mengurangkan dan menyerapkan tenaga kinetic yang berlebihan untuk melindungi pengguna dari kecederaan. Disebabkan oleh tujuan keselamatan ini, peranti penerapan daya hentaman diterokai. Kebiasaannya, kebanyakan tiub logam digunakan sebagai unsur penerapan daya hentaman. Tiub aluminium adalah salah satu jenis tiub logam yang diasasat dan dianalisis dalam projek ini. Satu idea telah dibangunkan dengan memperkenalkan kayu habuk sebagai bahan digunakan dalam peranti penyerapan daya hentaman. Projek ini telah dijalankan untuk mengkaji kesan kayu habuk dalam sifat keruntuhan dan tenaga penyerapan prestasi untuk meningkatkan peranti penyerapan daya. Tiga jenis tiub aluminium yang berbeza telah digunakan, iaitu tiub bulatan dan dua jenis berbeza saiz tiub segi empat dipenuhi dengan berbeza ketumpatan kayu habuk sebelum dimampatkan oleh daya kuasi-statik. Projek ini bermula dengan penyelidikan pengajian untuk memahami teori dan maklumat yang berkaitan dengan kajian masa kini. Selepas penyelidikan pengajian, didapati bahawa sifat-sifat bahan, sifat-sifat mekanikal dan saiz tiub amat memberi kesan kepada perubahan sifat bentuk dan tenaga penyerapan prestasi. Berikutan dengan ini, ujian tegangan dan ujian mampatan eksperimen telah dijalankan dalam projek ini. Ujian tegangan dijalankan untuk menyiasat dan menentukan sifat-sifat mekanikal pada tiub aluminium. Daripada hasil ujian tegangan yang diperoleh, sifat-sifat mekanikal ini akan digunakan untuk menilai teori beban purata. Manakala ujian mampatan eksperiment melibatkan persediaan ketumpatan kayu habuk yang dipenuhi di dalam tiub dan pemerhatian untuk tiub perubahan sifat bentuk. Kedua-dua aluminium tiub berongga dan tiub yang diisi kayu habuk telah dimampatkan dengan menggunakan INSTRON ujian mesin untuk mendapatkan persifatan daripada graf bebanan lawan keanjakan. Daripada graf bebanan lawan keanjakan, titik pepadatan, plastik gelombang kepanjangan, purata bebanan, tenaga penyerapan dan tenaga spesifikasi telah ditentu dan dianalisis. Teori pengiraan bagi purata bebanan, plastic gelombang kepanjangan dan tenaga penyerapan juga telah dinilai lalu dibandingkan dengan keputusan hasil daripada eksperimen. Kedua-dua keputusan hasil daripada eksperimen dan teori pengiraan menunjukkan bahawa kewujudan kayu habuk mendatangkan kesan kepada purata bebanan dan tenaga penyerapan.

ACKNOWLEDGEMENT

Throughout two semesters of the final year project, it would never have done without assistance of many fine individuals. Therefore, it is the opportunity to thanks all the people who help in the final year project.

First of all, among the people it is the great for me to express my deepest appreciation and thanks with gratitude to my final year project supervisor, Prof Dr. Md. Radzai bin Said, who is always giving all his effort during consultation to ensure the project is done and organized perfectly. His supervision, enthusiastic helps and guidance in this report greatly enhance me to do every task successfully.

Besides that, it is very special thanks to Prof Madya Dr. Azma Putra, the chairman of final year project, who always reminds us the date to submit the report and presentation in the group. The guideline on how to write the report and the important format for us to follow had been given by him. Because of it the progress report and the final draft report can be submitted before due date and the presentation slide also can be prepared early before the presentation.

At the same time, it is also thanks to En. Faizol Bin Kamarul Zahari, En. Wan Saharizal Bin Wan Harun and En Habirafidi Bin Ramly, the technicians from structural laboratory Faculty of Mechanical Engineering, En Ghazalan Bin Mohd Ghazi, the technician from Faculty of Manufacturing Engineering, for their advice, assistance and helpful in the fabrication and lab experimental works. Because of it, the experimental work by using the mechanical equipment can be completed successfully.

There are a lot of knowledge about the impact mechanics that I had learnt and gained during carrying out this final year project. All the knowledge is very precious to me because some of tools and machines are the first time for me to experience it. Some of the knowledge also I cannot obtain from reference books. Besides that, it is also thanks to the people that help me directly or indirectly to complete this final year project.

Lastly, it is also thanks to my mother, father and siblings due to their encouragement and supporting in this project and throughout this degree program.

TABLE OF CONTENTS

| CHAPTER | CONTENT | PAGE |
|------------------|---|----------|
| | DECLARATION | |
| | APPROVAL | |
| | DEDICATION | |
| | ABSTRACT | i |
| | ABSTRAK | ii |
| | ACKNOWLEDGEMENTS | iii |
| | TABLE OF CONTENTS | iv |
| | LIST OF TABLES | vii |
| | LIST OF FIGURES | ix |
| | LIST OF APPENDICES | xii |
| | LIST OF ABBREVIATIONS | xiii |
| | LIST OF SYMBOLS | xiv |
| CHAPTER 1 | INTRODUCTION | 1 |
| | 1.1 Background of study | 1 |
| | 1.2 Problem statement | 3 |
| | 1.3 Objectives | 3 |
| | 1.4 Scope of project | 4 |
| CHAPTER 2 | LITERATURE REVIEW | 5 |
| | 2.1 Description | 5 |
| | 2.2 Collapse behavior of plastic tubes filled with wood saw dust by A.A. Singace (2000) | 5 |
| | 2.2.1 Methodology | 6 |
| | 2.2.2 Theory | 6 |

| | | |
|------------------------------|---|-----------|
| 2.2.3 | Result and discussion | 7 |
| 2.3 | Quasi-static axial compression of thin-walled circular aluminium tubes by S.R. Guillow et. al. (2001) | 9 |
| 2.3.1 | Experimental procedure | 10 |
| 2.3.2 | Experimental result and discussion | 11 |
| 2.4 | Axial crushing analysis of tubes deforming in the multi-lobe mode by A.A Singace (1999) | 13 |
| 2.4.1 | Experimental set up | 14 |
| 2.4.2 | Results and discussion | 15 |
| 2.5 | Saw dust | 16 |
| 2.6 | Aluminium | 17 |
| 2.7 | Axial loading | 17 |
| 2.8 | Density | 18 |
| 2.9 | Mechanical properties | 19 |
| 2.10 | Deformation mode | 20 |
| 2.11 | Energy absorption | 24 |
| CHAPTER 3 METHODOLOGY | | 27 |
| 3.1 | Description | 27 |
| 3.2 | Flow chart | 28 |
| 3.3 | Material Preparation | 30 |
| 3.3.1 | Saw dust | 30 |
| 3.3.2 | Hollow Aluminium Tube | 31 |
| 3.4 | Preparation of tensile test coupon | 32 |
| 3.5 | Tensile test specimen fabrication | 33 |
| 3.6 | Tensile test experiment | 34 |
| 3.7 | Specimen and equipment preparation for axial compression experiment | 35 |
| 3.8 | Axial compression experiment | 38 |
| 3.9 | Capturing experimental result | 40 |

| | | |
|------------------|--|-----------|
| CHAPTER 4 | RESULT AND DISCUSSION | 41 |
| 4.1 | Description | 41 |
| 4.2 | Density of Saw Dust | 41 |
| 4.3 | Deformation characteristics | 46 |
| 4.3.1 | Circular tube deformation | 46 |
| 4.3.2 | Square tube deformation | 48 |
| 4.3.3 | Saw dust filled tube deformation | 53 |
| 4.4 | Tensile test result | 54 |
| 4.5 | Comparison of experimental results with theory | 55 |
| 4.5.1 | Theoretical calculation of plastic wavelength and mean load | 55 |
| 4.5.2 | Experimental results and of plastic wavelength and mean load | 59 |
| 4.5.3 | Comparison of mean load | 60 |
| 4.5.4 | Comparison of plastic wavelength | 63 |
| 4.6 | Load displacement characteristic | 65 |
| 4.7 | Energy absorption | 73 |
| CHAPTER 5 | CONCLUSION AND RECOMMENDATIONS | 76 |
| | REFERENCES | 78 |
| | APPENDICES | 82 |

LIST OF TABLES

| TABLE | TITLE | PAGE |
|-------|--|------|
| 2.1 | Type and size of wood filler with A and B wood constant. (A.A. Singace, 2000) | 6 |
| 2.2 | Theoretical and experimental mean crushing load of saw dust filled PVC tubes. (A.A. Singace, 2000) | 8 |
| 2.3 | Average crushing force of foam filled aluminium alloy tube (S.R. Guillow et.al. 2001) | 13 |
| 2.4 | Typical value of mechanical properties of pure aluminium | 19 |
| 3.1 | Description of materials used | 31 |
| 3.2 | Preparation of saw dust filled tube at different density | 37 |
| 4.1 | Calculation of saw dust density of circular tube (Length, $L = 100$ mm, Thickness, $t = 1.50$ mm, Outer diameter, $D = 25.3$ mm) | 43 |
| 4.2 | Calculation of saw dust density of square tube (Length, $L = 150$ mm, Thickness, $t = 1.10$ mm, External width, $c = 38.0$ mm) | 44 |
| 4.3 | Calculation of saw dust density of square tube (Length, $L = 150$ mm, Thickness, $t = 1.10$ mm, External width, $c = 50.6$ mm) | 45 |
| 4.4 | Tensile testing result of aluminium tensile test specimen | 54 |
| 4.5 | Theoretical and experimental mean crushing load of hollow tube | 60 |
| 4.6 | Theoretical and experimental mean crushing load of saw dust filled tube | 61 |
| 4.7 | Theoretical and experimental plastic wavelength of hollow tube | 63 |

| | | |
|------|--|----|
| 4.8 | Densification point, energy absorbed and specific energy of circular tube ($L= 100$ mm, $t= 1.50$ mm, $D = 25.3$ mm) at different density | 73 |
| 4.9 | Densification point, energy absorbed and specific energy of square tube ($L= 150$ mm, $t= 1.10$ mm, $D = 38.0$ mm) at different density | 74 |
| 4.10 | Densification point, energy absorbed and specific energy of square tube ($L= 150$ mm, $t= 1.10$ mm, $D = 50.6$ mm) at different density | 74 |



LIST OF FIGURES

| FIGURE | TITLE | PAGE |
|--------|---|------|
| 2.1 | Sectional photograph view of wood saw dust of PVC filled tube: (a) white wood; (b) red wood; (c) mixed wood (A.A. Singace, 2000) | 7 |
| 2.2 | Collapse deformation modes of circular 6060 aluminium tubes: (a) Axisymmetric mode; (b) Non-symmetric mode; (c) Mixed mode (S.R. Guillow et. al. 2001) | 9 |
| 2.3 | Experimental work using SHIMADZU universal testing machine (S.R. Guillow et. al. 2001) | 10 |
| 2.4 | Tensile stress strain curve of 6060 aluminium alloy (S.R. Guillow et. al. 2001) | 10 |
| 2.5 | Deformation mode of 6060 aluminium alloy circular tube: (a) Mixed mode; (b) Three sided non-symmetric folding; (c) Euler buckling (S.R. Guillow et. al. 2001) | 11 |
| 2.6 | Mode classification chart of 6060 aluminium alloy circular tube (S.R. Guillow et. al. 2001) | 11 |
| 2.7 | Comparison of the experimental result by S.R. Guillow and his team of average force with theory from Abramowicz and Jones. | 12 |
| 2.8 | Classical load displacement curve of tube deformed in axisymmetric mode | 14 |
| 2.9 | Classical load displacement curve of tube deformed in non-axisymmetric mode (Singace, 1999) | 15 |
| 2.10 | Saw dust material | 16 |
| 2.11 | Tube structure undergoes axial compression (Isabel, 2015) | 18 |

| | | |
|------|--|----|
| 2.12 | Circular tube deformed in concertina mode (Source: Bardi, 2006) | 20 |
| 2.13 | Folding behavior in square tube under quasi-static compression (Source: Ali Najafi & Masoud R.R., 2011) | 23 |
| 2.14 | Load displacement curve of tube crushing by axial loading (Source: Guillow and et al, 2001) | 25 |
| 2.15 | Load displacement graph of foam filled tube and empty tube (Source: Guillow and et al, 2001) | 26 |
| 3.1 | Flow chart of the project | 28 |
| 3.2 | Material and specimens used in experiment: (a) Saw dust; (b) Hollow circular aluminium tube; (c) Hollow square aluminium tube | 30 |
| 3.3 | Tensile test specimen dimensions from ASTM E8 standard. (ASTM, 2008) | 32 |
| 3.4 | Developed tensile test specimen using AutoCAD software | 32 |
| 3.5 | Laser cutting machine | 33 |
| 3.6 | Tensile test specimen after fabrication | 33 |
| 3.7 | INSTRON Universal Testing Machine | 34 |
| 3.8 | Indication marking of tensile test specimen | 34 |
| 3.9 | Band saw cutting machine | 36 |
| 3.10 | Weight balance | 37 |
| 3.11 | INSTRON 5585 testing machine in axial compression experiment | 38 |
| 3.12 | Video camera | 40 |
| 4.1 | Progressive axial crushing of circular tube (L= 100 mm, t= 1.50 mm, D= 25.3 mm) | 47 |
| 4.2 | Deformation pattern of circular tube (L = 100 mm, t = 1.5 mm, D = 25.3 mm) | 48 |
| 4.3 | Deformation pattern of square tube (L = 150 mm, t = 1.1 mm, c = 38.0 mm) | 49 |

| | | |
|------|---|----|
| 4.4 | Progressive axial crushing behavior of square tube (L=150 mm, t = 1.10 mm, c = 38.0 mm) | 50 |
| 4.5 | Deformation pattern of square tube (L= 150 mm, t= 1.1 mm, c= 50.6 mm) | 51 |
| 4.6 | Progressive axial crushing behavior of square tube (L=150 mm, t = 1.10 mm, c = 50.6 mm) | 52 |
| 4.7 | Breaking behaviour of square tube (L-150 mm, t= 1.10 mm, c = 50.6 mm) during quasi-static axial loading | 53 |
| 4.8 | Stress against strain curve from tensile test experiment | 54 |
| 4.9 | Illustration of determine mean load and plastic wavelength of circular tube (L = 100 mm, t = 1.5 mm, D = 25.3 mm) | 59 |
| 4.10 | Load displacement curve of axial crushing circular tube (L= 100 mm, t= 1.50 mm, D = 25.3 mm) | 65 |
| 4.11 | Load displacement curve of axial crushing square tube (L= 100 mm, t = 1.10 mm, c = 38.0 mm) | 67 |
| 4.12 | Load displacement curve of axial crushing square tube (L= 150 mm, t = 1.10 mm, c = 50.6 mm) | 68 |
| 4.13 | Load displacement curve of axial crushing circular tube (L= 100 mm, t= 1.50 mm, D = 25.3 mm) at different density | 69 |
| 4.14 | Load displacement curve of axial crushing square tube (L= 150 mm, t= 1.10 mm, c = 38.0 mm) at different density | 70 |
| 4.15 | Load displacement curve of axial crushing square tube (L= 150 mm, t= 1.10 mm, c = 50.6 mm) at different density | 71 |
| 4.16 | Photograph view of splitting square tube (L= 150 mm, t= 1.10 mm, c = 50.6 mm) | 72 |

LIST OF APPENDICES

| APPENDIX | TITLE | PAGE |
|----------|---|------|
| A1 | Gantt chart of PSM 1 | 82 |
| A2 | Gantt chart of PSM 2 | 83 |
| B1 | Progressive crushing of saw dust filled circular tube (L= 100 mm, t= 1.50 mm, d= 25.3 mm) | 84 |
| B2 | Progressive crushing of saw dust filled square tube (L=150 mm, t= 1.10 mm, c= 38.0 mm) | 85 |
| B3 | Progressive crushing of saw dust filled square tube (L=150 mm, t= 1.10 mm, c= 50.6 mm) | 86 |
| C | Tensile Test Specimen Dimension | 87 |
| D | Tensile Test Specimen Result Sample | 88 |
| E | Axial Compression Experimental Result Sample | 89 |

LIST OF ABBREVIATIONS

| | |
|------|--|
| IEA | Impact Energy Absorber |
| PVC | Polyvinyl Chloride |
| FFT | Foam-filled Tube |
| ASTM | American Society for Testing and Materials |
| CAD | Computer-Aided Design |
| LED | Light Emitting Diode |



LIST OF SYMBOLS

| | | |
|-------------------|---|---|
| P_{mm} | = | Theoretical mean crushing load |
| M_p | = | Full plastic bending moment per unit length |
| N | = | Number of lobes in multi-lobe collapse |
| D | = | Tube mean diameter |
| t | = | Tube wall thickness |
| P_w | = | Wood crushing load |
| σ_w | = | Wood strength |
| ρ | = | Average density of tested wood |
| ρ_s | = | Density of wood sawdust solidification state |
| F_{max} | = | Maximum axial force for first peak |
| F_{avg} | = | Average axial force |
| σ_{normal} | = | Normal stress |
| F | = | Internal force |
| A | = | Cross-sectional area |
| ρ_s | = | Density of filler |
| m_c | = | Combined mass of filler and volumetric cylinder |
| m_e | = | Mass of empty volumetric cylinder alone |
| V_o | = | Volume of filler displaced in the volumetric cylinder |

| | | |
|---------------|---|--|
| E | = | Modulus of elasticity |
| σ_{ys} | = | Yield strength |
| σ_{ut} | = | Ultimate tensile strength |
| P_{cr} | = | Critical load |
| K | = | Stiffness |
| L | = | Length |
| EA | = | Energy absorption |
| $F(\delta)$ | = | Instantaneous crush force with respect to displacement |
| c | = | Side length |
| D_o | = | Outer tube diameter |
| π | = | Pi |
| H_m | = | Half plastic wavelength |



CHAPTER 1

INTRODUCTION

1.1 Background of study

The deforming mode of empty and filled metal tubes subjected to axial loading is studied. Axial loading is applied until the deformation is formed at a characterised force magnitude. The deformation mechanism describes the instabilities of structure which leading to failure by a higher force beyond to the limit load (Bardi et al, 2006). In the present investigation, the collapse and axial crushing behavior of tubular structure is obtained from a series of experiments with considering to various properties such as length to diameter ratio, radius to thickness ratio, geometrical shape and material properties (Guillow et al, 2001). Besides that, the influence of filler in hollow tube also changes the modes of deformation and crushing behaviour.

Based on the past researchers, the foam-filled on the tubular structure has been studied analytically and experimentally, which brings saw dust into the investigation to determine its energy absorption and deformation characteristic. Saw dust is a solid residue, biodegradable and non-abrasive material usually produced in the timber industry. Saw dust is a wasted product, recyclable and cheap material thus it extracted and used to enhance the energy absorption capacity of tube (Singace, 2000). In application, saw dust are useful in manufacturing industry due to its mechanical and physical properties to produce insulators, multi plugs, mobile casings, accessories, hardboards, switchboards and automotive parts. Besides that, saw dust can be chemically treated to improve the tensile strength and water

absorption characteristics at the same time increase the biodegradability of polymer matrix composite (Hossain et al., 2014).

Tubes structures are one of establish passive energy absorbing equipment in the automotive, aerospace and transportation application. Different types of tubular absorbing structures are produced such as circular, triangular, hexagonal, honeycomb, foam filled and cellular. The most frequently used in energy absorber are square and circular tubes. Usually, metallic tubes are the majority consideration type due to manufacturing easiness and feasible. Comparing between the structures, aluminium circular tubes are greatly used as energy absorbing structures due to the structure has low density, high strength and well deformability (Emin, 2016). Besides that, filled tube structure is also greatly used in car front bumpers and front beam (Gan, 2016).

In mechanics, axial loading is a force that is directed along the longitudinal axis of the member. Axial loading tends to elongates or shorten a member are termed tension force and compression force respectively. During axial loading applied, stress acts on the surface that is perpendicular to the direction of the internal force (Timothy, 2014). Under axial loading, deformation and collapse mode usually occurred on the tubes structure during crashing event. Axial and bending collapses are the classical types of collapse mode (Liu et al, 2015). Quasi-static and dynamic loading are the types of axial loading.

1.2 Problem statement

Nowadays, the importance of personal safety and protection from impact has been concerned in the safety application. The research and development on impact energy structure has been studied earlier, especially for automotive industries to design the various types of vehicles. Impact energy absorber (IEA) is one of the important mechanical structural components used in this application eliminating and reducing the excessive kinetic energy when the collision is occurred. In order to achieve the quality for this application, the installed IEA device has to attain its crashworthy performance. Due to this purpose, the IEA device is studied in this project. To study the impact energy absorption (IEA) device, metal tube is used as the medium to evaluate and analyse its deforming mode, energy absorption characteristics and compare the results with theory. Besides that, metal tube is also inserted with the filling material to study and analyse deformation characteristics as well. It is expected that the material filled tube would have higher crashworthiness in this project.

1.3 Objectives

The aim of the project is as followed:

- i. To observe and study the deforming mode of circular and square aluminium tube under axial loading.
- ii. To determine the mean load and plastic wavelength of circular and square aluminium tube and compare with the theory.
- iii. To study the load-displacement characteristics and the energy absorption of empty and saw dust filled circular and square aluminium tube.

1.4 Scope of project

The experimental project will focus on the deforming mode, mean load, plastic wavelength, load-displacement characteristic and the energy absorption performance of empty and saw dust filled of circular and square aluminium tube under axial loading. Besides that, the experimental project will also focus on comparing three types of densities of saw dust filled of the circular and square aluminium tube under axial loading. The other aspects such as the cost and will not be covered in this project.



CHAPTER 2

LITERATURE REVIEW

2.1 Description

This chapter provides the previous studies and relevant information related to the present of the study. In this chapter, the related resources such as past experimental works, properties of material and deformation information are reviewed. Besides that, the sources from other researchers such as journal and the technical reports are also selected to be studied before conducting the experiment. The theoretical studies obtained from the previous study will be compared with the present of experimental result.

2.2 Collapse behavior of plastic tubes filled with wood saw dust by Singace (2000)

This is an experimental work by using quasi-static loading to study the effect of wood filler on the deformation mode and the energy absorption of PVC tubes. Compression test was carried out by using universal testing machine to obtain the mechanical properties and then validated by the theoretical model. Theoretical calculation such as mean crushing load was compared with the experimental result.

2.2.1 Methodology

The experimental crushing test was set at 10 mm/min loading rate. Redwood, white wood and mixture of red wood and white wood at different densification were filled into the tube. Besides that, the mechanical properties of the wood saw dust was examined by conducting the compression test the three type of wood at various masses.

2.2.2 Theory

The theoretical mean crushing load in this journal study is given in equation 2.1

$$P_{\text{mm}} = M_P \left(-\frac{\pi}{3}N + \frac{2\pi^2}{N} \tan\left(\frac{\pi}{2N}\right)\frac{D}{t} \right) \quad (2.1)$$

The mean crushing load of own wood is given in equation 2.2

$$P_w = \frac{\pi}{4} D^2 \sigma_w \quad (2.2)$$

where σ_w is given in equation 2.3

$$\sigma_w = A \sigma_{ws} \exp\left(0.5 \left(\frac{P}{P_s}\right)^B\right) \quad (2.3)$$

where σ_{ws} is the compression stress of wood dust at solidification state with value of 4 MN/m² and A and B are wood grade constant as shown in Table 2.1.

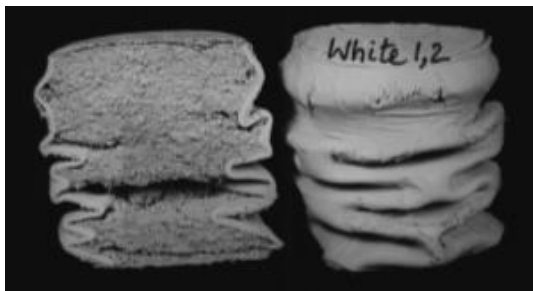
| No. | Type of wood and (size) | A | B |
|-----|-------------------------|-------|-------|
| 1 | White sawdust (1,-) | 0.874 | 0.725 |
| 2 | Red sawdust (1,-) | 0.974 | 0.764 |
| 3 | Mixed sawdust (1,-) | 0.93 | 0.723 |
| 4 | White wood chips (2,-) | 0.852 | 0.554 |
| 5 | Red wood chips (2,-) | 0.78 | 0.713 |
| 6 | Mixed wood chips (2,-) | 0.787 | 0.536 |
| 7 | White wood chips (3,-) | 0.9 | 0.84 |
| 8 | Red wood chips (3,-) | 0.96 | 0.854 |
| 9 | Mixed wood chips (3,-) | 0.871 | 0.654 |

Table 2.1: Type and size of wood filler with A and B wood constant
(Singace, 2000)

2.2.3 Result and discussion

From the experimental result, there is no variation of initial collapse load between wood dust filled PVC tubes. Due to the presence of wood saw dust, progressive compression loading increased the overall mean load to shortening the tube. As the wood saw dust upon applied force, the internal pressure of tube wall increases, causing the load to collapse also increases. Density alters as the axial loading progress. As the axial loading progress until the end, wood saw dust become locked state like a solid wood. In the load displacement graph, curve begins with first high peak and then followed by elevated peaks when the wood saw dust within the tube becomes denser. When the wood saw dust become denser, the axial crushing load of PVC tubes increases with an observable reduction throughout in tube shortening.

For white wood saw dust filled tube, tube formed multi-lobe mode firstly and then shifted into concertina mode. However, white wood chips filled tube shifted only to concertina mode in the end of densification. For red wood saw dust filled tube, the degree of peak load rises with the formation of concertina ring mode. For mixed saw dust of red and white wood, tube formed identical behavior, with transitional between in red wood and white wood. Figure 2.1 shows the sectional photograph view of wood saw dust of PVC filled tube.



(a)



(b)



(c)

Figure 2.1: Sectional photograph view of wood saw dust of PVC filled tube: (a) white wood; (b) red wood; (c) mixed wood
(Singace, 2000)

On the other hand, the theoretical mean crushing load of wood saw dust filled PVC tubes are determined from equation 2.4.

$$P_{mm}^w = P_{mm} + P_w \quad (2.4)$$

Table 2.2 shows the theoretical and experimental mean crushing load of saw dust filled PVC tubes.

Table 2.2: Theoretical and experimental mean crushing load of saw dust filled PVC tubes.
(Singace, 2000)

| No. | Specimen | ρ/ρ_s^a | P_w Eq. (9) | P_c Eq. (4) | P_{mm} Eq. (1b) | P_{mean} Eqs. (10) or (14) | P_{exp} |
|-----|-----------|-----------------|------------------|------------------|----------------------|------------------------------------|-----------|
| 1 | White 1,2 | 0.1529 | 15.38 | ^b | 6.85 | 11.12 | 11.34 |
| 2 | White 1,5 | 0.2161 | 15.87 | 14.03 | 6.85 | 12.25 | 16.89 |
| 3 | White 2,3 | 0.2110 | 16.79 | ^b | 6.85 | 11.82 | 9.50 |
| 4 | Red 1,1 | 0.1715 | 16.94 | 13.28 | 6.85 | 12.36 | 11.25 |
| 5 | Red 1,3 | 0.1716 | 16.95 | 13.28 | 6.85 | 12.36 | 13.59 |
| 6 | Red 2,2 | 0.2246 | 14.30 | ^b | 6.85 | 10.58 | 11.00 |
| 7 | Red 2,4 | 0.1454 | 13.74 | 12.87 | 6.85 | 11.15 | 12.09 |
| 8 | Mix 1,2 | 0.1761 | 16.55 | ^b | 6.85 | 11.70 | 11.11 |
| 9 | Mix 1,5 | 0.1675 | 16.48 | 13.21 | 6.85 | 12.18 | 16.91 |
| 10 | Mix 2,1 | 0.2497 | 15.96 | ^b | 6.85 | 11.41 | 9.93 |
| 11 | Mix 2,5 | 0.1725 | 15.35 | 13.29 | 6.85 | 11.83 | 11.21 |

^a $\rho_s=750 \text{ kg/m}^3$.

^b No collapse in concertina mode.

2.3 Quasi-static axial compression of thin-walled circular aluminium tubes by Guillow et. al. (2001)

This is an investigation for further experimental work in axial compression for hollow circular tubes. 70 quasi-static experimental tests had been conducted on circular 6060 aluminium tubes. The comparisons had been made between the theories and the experimental results for average crushing force. From the experiment, researchers discovered that the F_{\max}/F_{avg} ratio increases with the D/t ratio. Some collapse deformation modes had been studied by them as shown in the Figure 2.2.

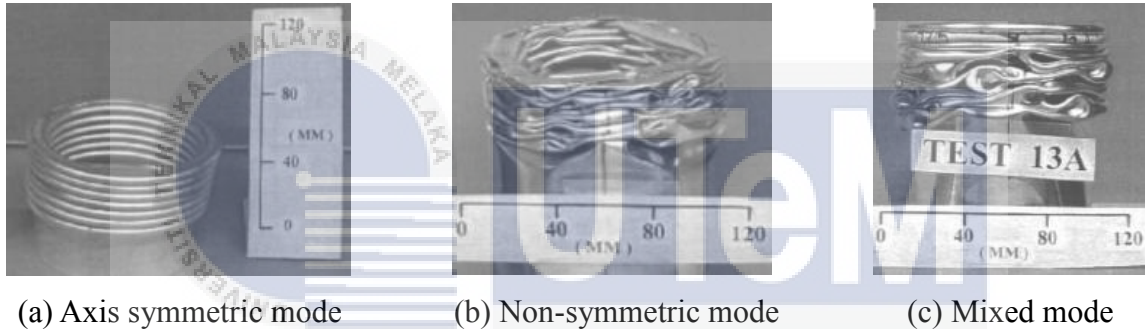


Figure 2.2: Collapse deformation modes of circular 6060 aluminium tubes: (a) Axisymmetric mode; (b) Non-symmetric mode; (c) Mixed mode
(Guillow et. al. 2001)

2.3.1 Experimental procedure

The experiment work was carried out by using SHIMADZU universal testing machine where the flat end platens were used during axial loading as shown in the Figure 2.3.

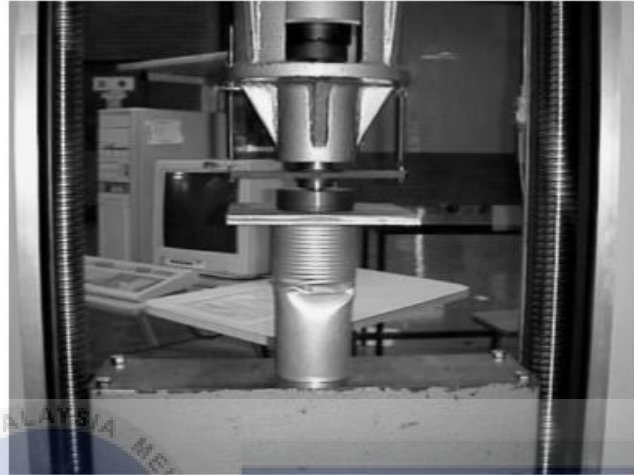


Figure 2.3: Experimental work using SHIMADZU universal testing machine
(Guillow et. al. 2001)

The strain rate was set to be 5 mm/min. To obtain the experimental data for evaluation, they use LABTECH data-logger. Before the experiment work started, they had done several tensile testing to obtain the mechanical properties of material 6060 aluminium alloy. Figure 2.4 shows one of the tensile stress strain curve of material 6060 aluminium alloy conducted by them.

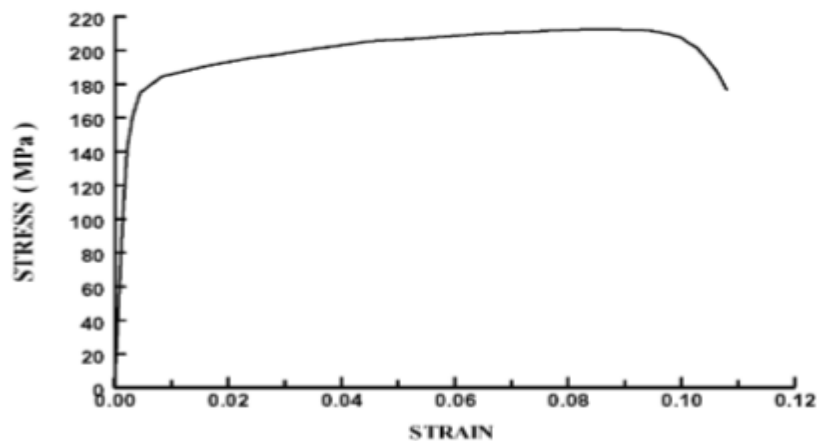
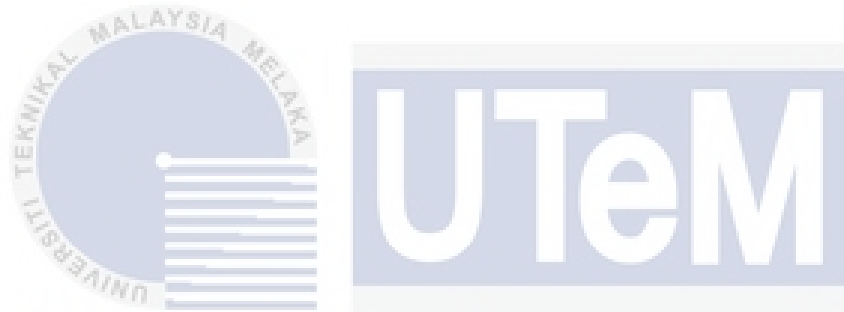


Figure 2.4: Tensile stress strain curve of 6060 aluminium alloy
(Guillow et. al. 2001)



اونيورسيتي تيكنيكل مليسيا ملاك

UNIVERSITI TEKNIKAL MALAYSIA MELAKA

The comparison between the experimental with non-symmetric mode and theoretical calculation for average crushing force were agreeable at $D/t > 100$. Guillow and his team had calculated that the average crushing force using axis-symmetric equation was lower as compared with their experimental results. However by using non-symmetric equation, they calculated the average forces were higher than their experimental result which is indicated as shown in the Figure 2.7.

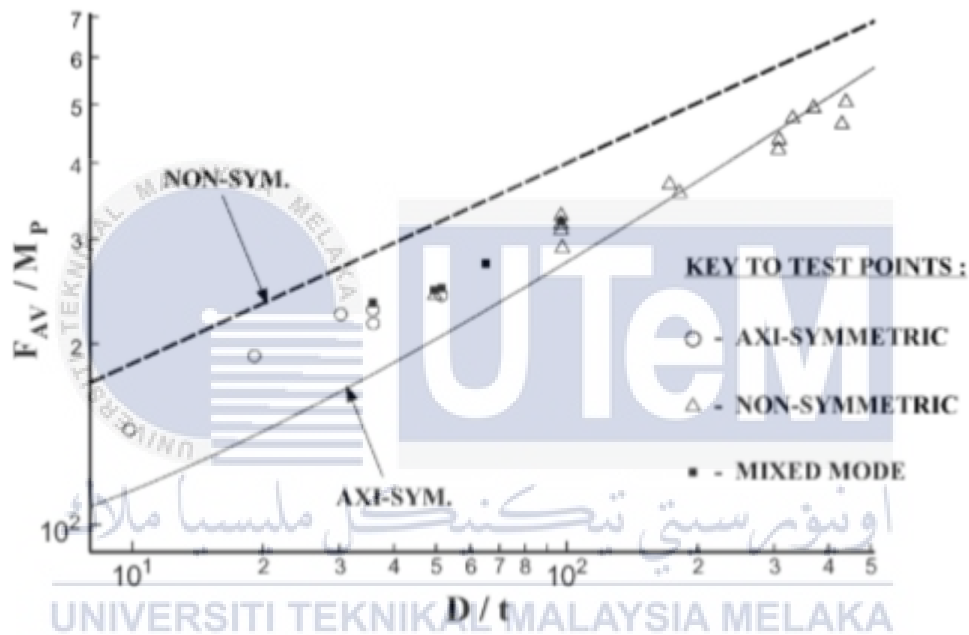


Figure 2.7: Comparison of the experimental result by S.R. Guillow and his team of average force with theory from Abramowicz and Jones.

As for the analysis, the average force predicted from theory with the experimental work done by them declared two significant aspects. The first aspect was the theoretical average force using different collapse modes was largely apart from each other. The secondly was the dependence of D/t ratio on average crushing force. For S.R. Guillow and his team experimental work, the average crushing force was dependent on $(D/t)^{0.32}$; however for theory the average crushing force was $(D/t)^{1/2}$ in axis-symmetric mode.

S.R. Guillow and his team predicted the average crush force increases as the aluminium alloy tube filled with foam. Table 2.3 shows the experimental work for average crushing force for foam filled aluminium alloy tube by S.R. Guillow and his team.

Table 2.3: Average crushing force of foam filled aluminium alloy tube
(S.R. Guillow et.al. 2001)

| Foam density (kg/m ³) | F_{AV} for foam only (kN) | F_{AV} for empty aluminium tube (kN) | Sum of two columns at left (kN) | F_{AV} for foam filled A1 tubes (kN) |
|--------------------------------------|-----------------------------------|--|---------------------------------------|--|
| 35 | 0.908 | 15.53 | 16.44 | 19.32 |
| 60 | 2.685 | 15.53 | 18.22 | 21.10 |
| 140 | 12.43 | 15.53 | 27.96 | 28.45 |

They suggested that foam contribute support to the tube which increases the crushing force. Besides that, they also find out that foam filled tube influences the tube collapse mode. For 60 kg/m³ foam density, the filled aluminium tube deformed in mixed mode while for 140 kg/m³, the filled aluminium tube deformed in axis-symmetric mode.

2.4 Axial crushing analysis of tubes deforming in the multi-lobe mode by A.A Singace (1999)

This is an experimental research focuses on the crushing load of tube collapse deformed in multi lobe mode. The study generates eccentricity factor, which is the function of tube geometry and number of lobes to determine mean collapse load. Singace described that for tube at end constraint, first fold usually produced at one end of the tube and then followed by radially outward deformation. Plastic hinge will formed at a certain distance from end of tube. For fixed end tube, plastic hinge will formed adjacent to the constrained edge. He stated that when the tube is compressed, inward forces produced radially inward by the hoop stress to expand the tube radially outward.

Singace suggested that the first buckle of tube is always outwards and begins with axisymmetric collapse mode. When the load is progressed, axisymmetric fold will change to non-axisymmetric mode or proceed with axisymmetric mode depend on the material properties and geometric ratio. Circumferential plastic hinge is formed to promote axial bending and hence folding is produced. In non-axisymmetric mode, circular tube would form triangular fold, from which tube wall would make angle inward at the base. During the first folding, initially the end of the tube shift inwards, which leads to partially inside and partially outside about the tube.

2.4.1 Experimental set up

Singace built up the experimental testing by using metal tubes which were made up of brass, copper and aluminium alloy. The metal tubes were crushed by using universal testing machine at rate of 5 mm/min. The classical load displacement curve for tubes deformed in axisymmetric mode and non-axisymmetric mode are as shown in the Figure 2.8 and Figure 2.9.

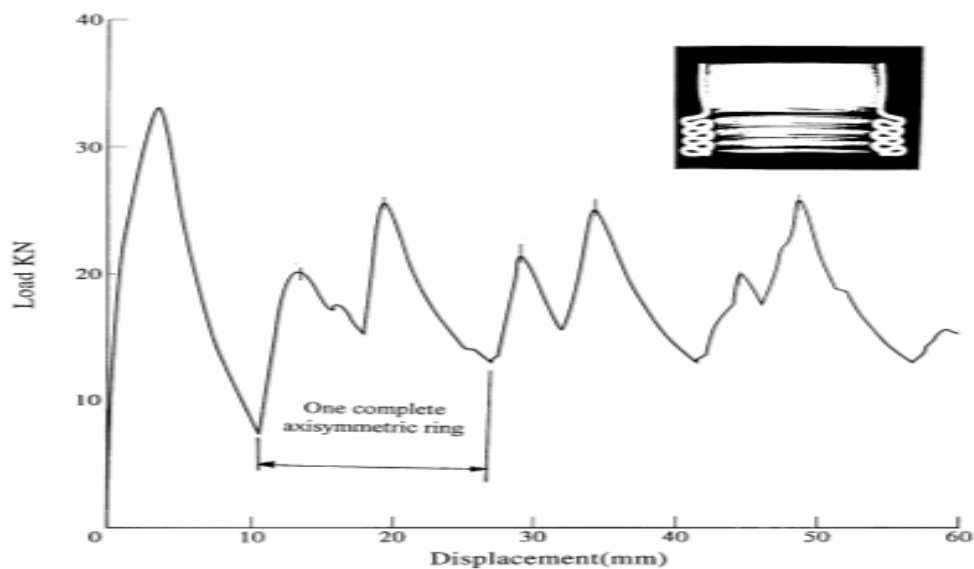


Figure 2.8: Classical load displacement curve of tube deformed in axisymmetric mode

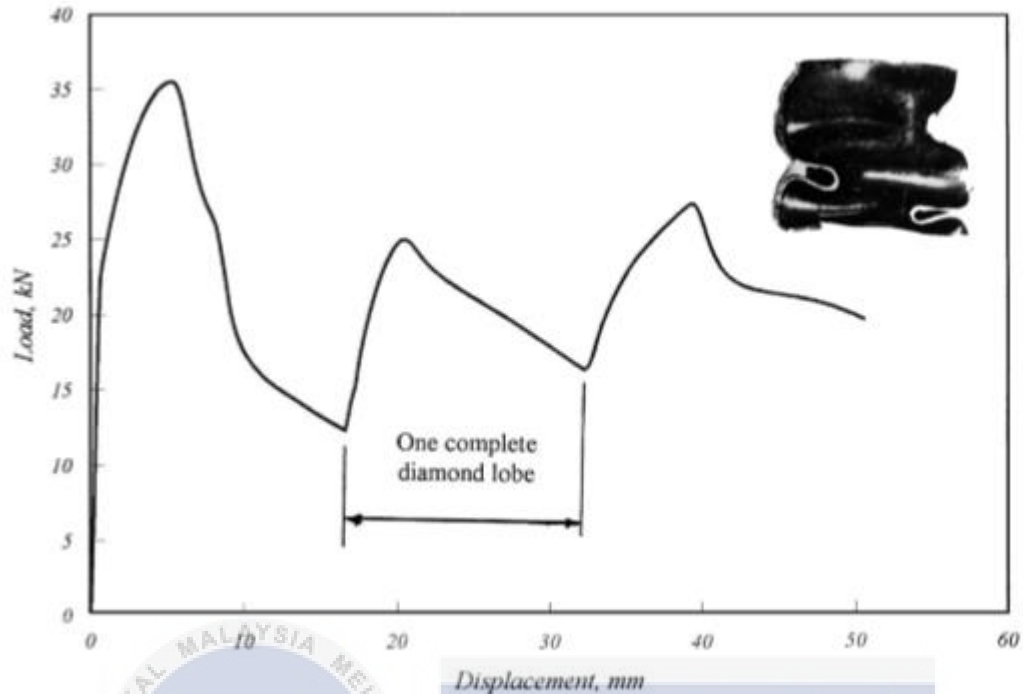


Figure 2.9: Classical load displacement curve of tube deformed in non-axisymmetric mode (Singace, 1999)

2.4.2 Results and discussion

Singace pointed out that the load displacement curve for tube deformed in axisymmetric mode was represented by first high peak load and then followed with repeated high and low peak loads which resemble to one complete ring fold. The repeated high peak load was for inward folding and the low peak load was for outward folding. However the inward and the outward part of multi-lobe fold produced circumstantially and thus they are resemble to both inward and outward folding. For tube deformed in non-axisymmetric mode, load displacement curve was represented by first high peak load and then followed by repeated low peak load. The successive formation of two low peak loads represented one complete diamond fold.

2.5 Saw dust

Saw dust is the small chippings residue produced by sawing of wood tree. Saw dust is available by-product from natural resources from the wood industry as a waste by mechanical processing of raw wood in the sawing process. Figure 2.10 shows the saw dust material.



Figure 2.10: Saw dust material

In chemical composition, saw dust is composed of carbon, hydrogen, oxygen, and nitrogen (Bachir, 2012). Saw dust is light, readily obtainable and biodegradability makes it as the addition material to provide better combinations in the building and automobile sector (Takian, 2013).

On the other hand, saw dust has a better mechanical property in term of frictional interaction and particle size distribution. In term of frictional interaction, the behaviour is described by friction coefficient between the particles and internal tube surface. Friction coefficient described the tangent of linearized relationship between shear stress and normal stress during sliding of particles against the construction material surface. The interaction between saw dust and internal tube surface during operation is crucial factor to attain stability in mechanical process. In term of particle size distribution, a smaller particle size decreases the relative displacement between particles. The smaller particle size resulted decrease the compressibility due to higher cohesive force and interlocking between the particles (Mateusz et al, 2015).

Since saw dust acts as a filler material, the combination of the tube structure and the filler give the advantage in the crushing efficiency. The interaction effect between the filler and the tubular wall provides enhancement in the mechanism, which leads to a higher energy dissipation. At the same time, the presence of the filler material also stabilizes the whole irregular warping pattern of the empty shape tube and led to enhance the efficiency in term of energy absorption (Seitzberger et al, 2000). The deformation behaviour also improves the ductility and delaying the failure (Isabel et al, 2015).

2.6 Aluminium

Aluminium is the nonferrous metal usually obtained in rock materials, which it exists as alumino silicates. The outstanding characteristics of aluminium are light weight, resistance to corrosion, and high thermal and electrical conductivity. Aluminium is the most versatile materials which it can be casted, extruded, machined, brazed and welded. Aluminium consists of thin-oxide coating which can prevent from the corrosion. Generally, aluminium is usually alloyed with copper, silicon, manganese, magnesium and zinc to increase the stiffness and strength (Richard, 2015).

2.7 Axial loading

When an axial loading applied, stress acts on the surface that is perpendicular to the direction of the internal force. This type of stress is called as normal stress. The magnitude of the normal stress can be determined from the relationship between the intensity of internal force and the cross section area, where it is given in equation 2.5.

$$\sigma_{\text{normal}} = \frac{F}{A} \quad (2.5)$$

When the structure is subjected to tension and compression, the potential energy in the molecules of the object is converted to mechanical energy. Tension is the axial force that leads to lengthen a structure, while compression is the force that leads to shorten the structure. Both tension and compression causes the strain and failure of the structure depends on the magnitude of force applied and the cross-sectional area of object (Timothy, 2014). Figure 2.11 shows the tube structure undergoes axial compression.



Figure 2.11: Tube structure undergoes axial compression

(Isabel, 2015)

2.8 Density

One of the important properties which affect the strength property is the density. Density increases the load applied to tube structure, which leads to affect its mechanical properties. From the literature study of researchers, the stiffness value of mechanical properties in foam-filled tube (FFTs) increases by increasing the density of the foam filler. When load transfers from tube to filler, compressive response will be improved between the tube wall and filler. Besides that, the filler foam with density of tube also improves in the peak stress and energy absorption. Compared to empty tubes, the presence of the filler in the tube decreases the stress drop magnitude (Isabel et al, 2015).

Typically, density enclosed in the tube can be calculated by adding the filler into a volumetric cylinder to reach the marked volume; while its weight could be determined by subtracting the combined mass of filler and volumetric cylinder with the mass of empty

volumetric cylinder alone. The density of filler is calculated based on the formula as shown in equation 2.2 below (Rizki, 2010).

$$\rho_s = (m_c - m_e) / V_o \quad (2.6)$$

where ρ_s is the density of filler

m_c is the combined mass of filler and volumetric cylinder

m_e is the mass of empty volumetric cylinder alone

V_o is the volume of filler displaced in the volumetric cylinder

2.9 Mechanical properties

Aluminium material has significant effect on the mechanical properties of metal. Table 2.4 shows the typical value of mechanical properties of aluminium such as Modulus of elasticity, yield strength and ultimate tensile strength. This value is useful when the tube is subjected to axial loading.

Table 2.4: Typical value of mechanical properties of pure aluminium

| Metal | Modulus of elasticity, E | Yield Strength, σ_{ys} | Ultimate Tensile Strength, σ_{ut} |
|--------------|---------------------------------|---|--|
| Aluminium | 71.7 GPa | 11 MPa | 90 MPa |

Young's Modulus is the measure of the stiffness of a material, which it determines the strength of material can withstand the amount of load. Yield strength is the stress that induces a specified permanent set in the material. In stress-strain diagram, the yield strength is determined through a line draw parallel to the determined specified permanent. However, tensile strength corresponds to the maximum stress reached on the stress-strain diagram (Richard, 2015).

2.10 Deformation mode

Deformation is caused by an applied load to the body. Consequently, deformation changed the size and the shape of the structure under loading that varies with position and orientation. Under loading condition, deformation will be varying throughout the body. Some segments will experience stretching, while others will experience contractions (Timothy, 2014). In this literature study of deformation, concertina mode, diamond mode, buckling and plastic folding are the non-uniform nature of load-induced deformations mode.

In the compressive of tubes under axial loading, the specimen initially deforms in the weakest region. The collapse behaviour of circular tube is generally depending on the ratio of diameter to thickness, D/t . For a lower diameter to thickness ratio D/t , tube would deform in concertina mode. Concertina mode is defined as axisymmetric mode occurred in the thicker tube. Figure 2.12 shows a circular tube deformed in concertina mode.



Figure 2.12: Circular tube deformed in concertina mode.

(Source: Bardi, 2006)

For a higher ratio of diameter to thickness ratio D/t , tube would deform in diamond mode. Diamond mode is defined as non-axisymmetric mode occurred in the thinner tube.

Circular tube is an useful energy absorbing component subjected to progressive collapsing and deformation in axisymmetric concertina, diamond and mixed mode, depended on the mean diameter and its thickness (Gupta, 1998). Based on other researcher, non-asymmetrical mode will be the prevailing mode for circular tubes of $R/t < 100$ for aluminium, copper and stainless steel tube. The wall of tube will be deformed into the triangles shape around the circumference of tube (Singace, 1999).

Nevertheless, once the length of the tube is higher than its critical length, Euler buckling mode would be deformed. Buckling is described as when a structure starts to deform laterally, the deflection grows larger and causes to catastrophic failure. The deformation mode occurred rashly when a slightly increase of load is applied. This type of deforming mode is mostly caused by compressive axial force which causes structure bend unexpectedly. When the buckling is occurred, a relatively great lateral deflection is produced by a small increase in compressive load. Buckling failure is illustrated as stability failure where the structure changed from a stable equilibrium state to unstable state (Timothy, 2014).

Buckling deformations usually started from the arising dented area from which the dent initiates at the ends towards the sides. Once the load is increased, dented area is further deepen and developed until it encompassed into half the circumference approaching the dent. However same phenomenon occurred on the area at the buckled zone, where bulge was produced at the side opposite to the dent occurred exactly at the location at which the specimen buckled (Tohid et al, 2015).

The nature of buckling is related with the concept of stability of equilibrium. When the axial load is applied, upsetting moment is created at the structure that tends to cause column to moves away from its initial position. Besides that, there is a restoring moment produced which tends to return the system to its initial orientation. When the restoring moment is greater than

the upsetting moment, the system will tend to return to its original configuration. However once the upsetting moment is larger than the restoring moment, the system is unstable which cause the column collapses (Timothy, 2014).

The concept of stability and instability of the structure can be investigated by determining the magnitude of axial load, which is called critical load, P_{cr} . The critical load, P_{cr} is the maximum magnitude to cause buckling and it occurs when the restoring moment is equal to the upsetting moment. When the load applied to the structure is lower than P_{cr} , the system is stable thus buckling would not occur. However when the load applied is greater than P_{cr} , the system is not stable hence buckling would be occur. To enhance the stability of the structure, where the critical load must be increased to prevent buckling occur. The methods are by increasing the stiffness, K or by decreasing the length, L of the structure (Timothy, 2014). The relationship between the critical load, P_{cr} , stiffness, K and length, L are indicated as shown in the equation 2.7.

$$P_{cr} = \frac{4K}{L} \quad (2.7)$$

When the yield stress is exceed, the structure started to yield and the folding is formed. Plastic folding involved inward and the outward folding which occur concurrently. The number of the fold and the localization of the initial folding layer depend on the geometrical parameters such as wall thickness, diameter, height and the material characteristics.

Usually, empty tube starts to deform in the weak region. When the tube is compressed, the tube wall is likely to displace radially outwards. From there, an outward force is produced, which pushing outward radially of the tube. In between the testing machine platens and the end of the tube, there is a frictional forces acting to oppose the movement at the end of the tube, causing the afterwards tube wall initiates the first outward warping. At one of the two

ends of the tube, the first fold is started and then facilitated by a radially outward movement. At the same time, inward movement is also created by the hoop expansion of radially outward movement of force. When the compression loading is increased, first fold is formed and the plastic bending hinge is produced at the restriction edge. As the loading is progressed after the first folding is completely formed, more deformation is extended. The stress increases again which leads to formation of the second fold. The process is repeated constantly, while the peaks of the stress in the load displacement diagram represent the number of folds (Singace, 1999). Figure 2.13 shows a folding behavior in square tube under quasi-static axial compression.

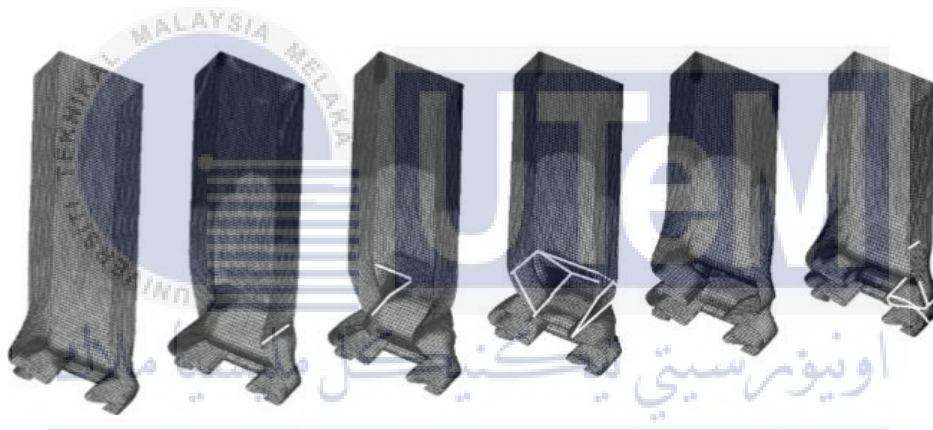


Figure 2.13: Folding behavior in square tube under quasi-static compression
(Source: Ali Najafi & Masoud R.R., 2011)

The folding initiates at one end of the tube in concertina mode whereas in diamond mode the folding accompanies with the change in cross sectional shape of the tube (Andrews et al, 1983). In load displacement diagram of concertina mode, high peak of curve corresponds to an inward folding and the next low peak of curve corresponds to an outward folding. When a successive folding is produced, plastic bending hinge formed at a certain distance from the end of the tube. After the symmetric folding is completely compressed, the stress is then increases again (Singace, 1999).

2.11 Energy absorption

Work done performed by axial loading causes the structure to deform is related to the principle of conservation of energy, where the energy transformed from one state to another. Work done by the axial loading is transformed into the energy absorbed in the strains of the structure (Timothy, 2014). However, the energy absorption is concerned with the factors such as material properties, geometrical shape and impact loads. Different materials and various geometrical shapes exhibit different capability of energy dissipation due to its high ratio of strength to weight and its stability of destruction pattern (Ying and et al, 2016). Based on the previous experimental work by the researchers, concertina mode has a higher degree of plastic deformation than diamond mode thus causing the energy absorption in concertina mode is greater than in the diamond mode (Andrews and et al, 1983).

When a structure deforms as a result of applied loads, work is done on the body by the loads. As the deformation occurs in the body, energy is absorbed in the body as strain energy. Therefore, energy absorption is described as the work needed to produce the collapse mode. The energy is initially changed into elastic strain energy in the deformed tube and then dissipated into plastic deformation during collapse (Andrews and et al, 1983). The energy absorption performance of the tube structure by axial loading can be characterized by a load displacement diagram. Figure 2.14 shows the load displacement curve for tube crushing by axial loading.

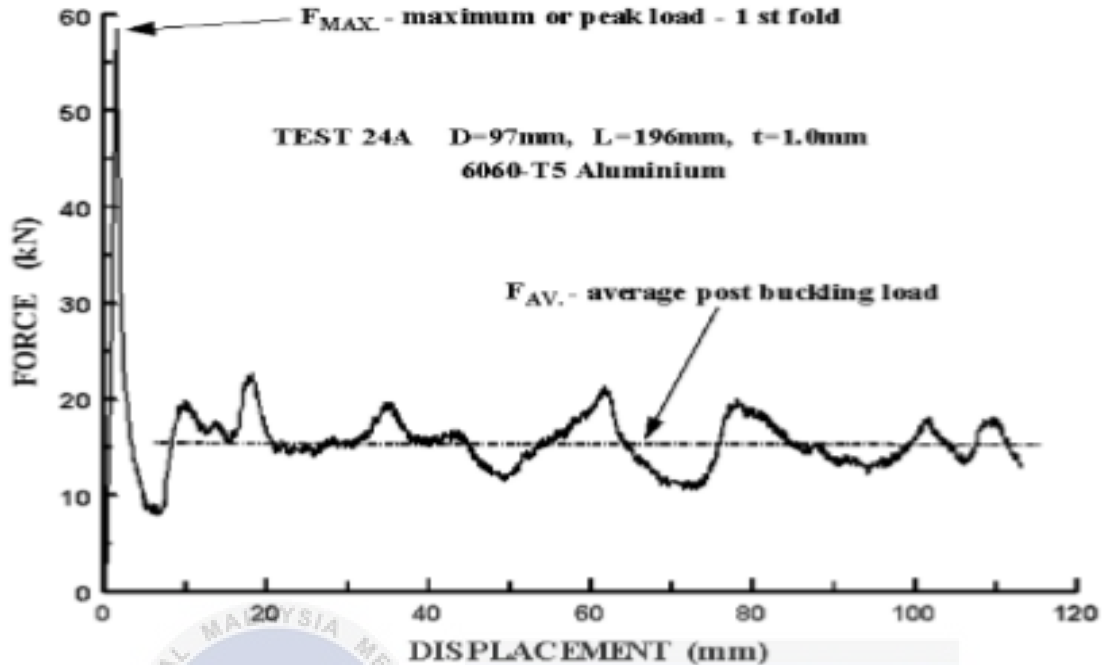


Figure 2.14: Load displacement curve of tube crushing by axial loading
(Source: Guillow and et al, 2001)

To study the load displacement characteristics, various parameters are used such as peak load, total energy absorption, specific energy absorption and mean crush force. Peak load is the maximum force needed to originate collapse, deformation and energy absorption process (Emin et al, 2016). On the other hand, energy absorption is meant as the energy needed to cause the structure failure (Andrews and et al, 1983). The energy absorption is given by the formula as shown in the equation 2.8.

$$EA = \int_0^{\delta} F(\delta) d\delta \quad (2.8)$$

where $F(\delta)$ is the instantaneous crush force with respect to the displacement δ

The specific energy absorption is the ratio of the energy absorption to the mass of the structure (Gan et al, 2016). The specific energy absorption is shown in the equation 2.9.

$$\text{Specific Energy Absorption} = \frac{\text{Energy Absorption}}{\text{Mass}} \quad (2.9)$$

Based on the researchers stated, the energy absorption increased with the number of corners of metallic tubes (Rafea and et al, 2017). Besides that, the energy absorption, mean crushing force and peak crushing force also increased with filler density and the diameter to thickness ratio. Filler in the tube contains of air gap which giving an improvement in the mechanical response to the structure when subjected to loading modes. Filler also retains the deformation of the tubes through a system which change to increase the ductility and delaying the failure. The existence of the filler takes an advantage which contributing in term of failure modes with a much more stable crushing manner. Load transfer from the tube's inner wall to the filler in the composite structure results in better mechanical properties and a higher energy absorption capacity (Isabel and el al, 2015). Figure 2.15 shows the load displacement graph which characterizes the effect of foam filler under axial loading. The energy absorption of the foam filled tube is higher than the empty tubes.

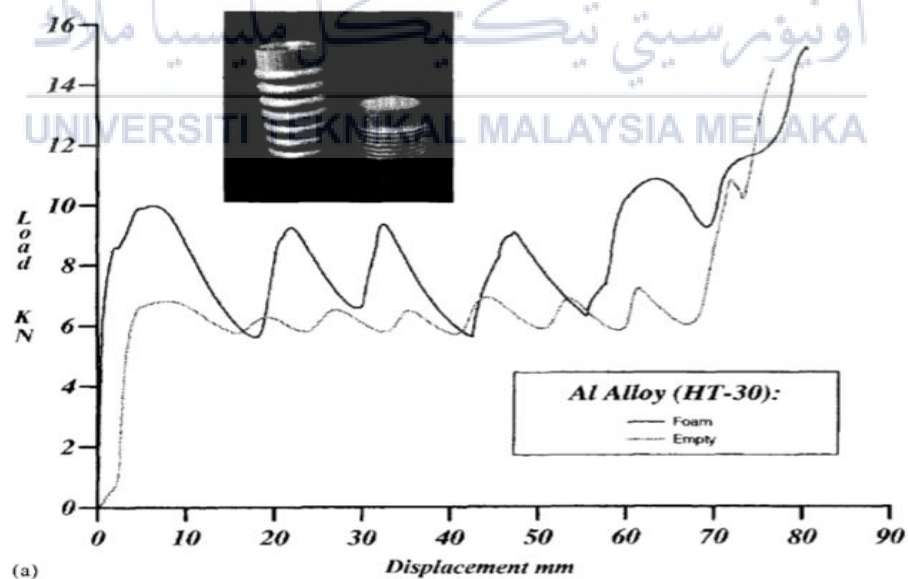


Figure 2.15: Load displacement graph of foam filled tube and empty tube

(Source: Guillow and et al, 2001)

CHAPTER 3

METHODOLOGY

3.1 Description

This chapter provides the methods, procedures and materials of the experimental work. In conducting the experiment, the physical measurement, apparatus and equipment used for axial compression test is summarized in this section. Each steps and process involved in this experiment will be discussed such as specimen preparation, specimen fabrication, tensile test and compression test. Before experimental work is carried out, tensile test experiment was done to determine the mechanical properties of materials.

Axial compression test was carried out by using three types of metal tube at different dimension. Hollow metal tube was compressed first in the beginning of experiment, followed by saw dust filled metal tube at three different densities. Next, hollow and filled metal tube were weighted and labelled in this experiment. On the other hand, the INSTRON testing machine, video camera supported with a tripod and suitable lighting were set up in beginning of experiment to enable tube deformation captured.

During the experimental work carried out, load displacement curve was plotted by the system of the INSTRON testing machine. For each displacement interval, voice was uttered out and the deformation behaviour of metal tubes was recorded by the video camera. After the experiment, the metal tube was weighted again and the deformed tubes lengths were recorded in the report. The general methodology of the experiment was summarized in the flow chart as shown in Figure 3.1.

3.2 Flow chart

Flow chart in Figure 3.1 described the briefly whole process of the experiment step by step.

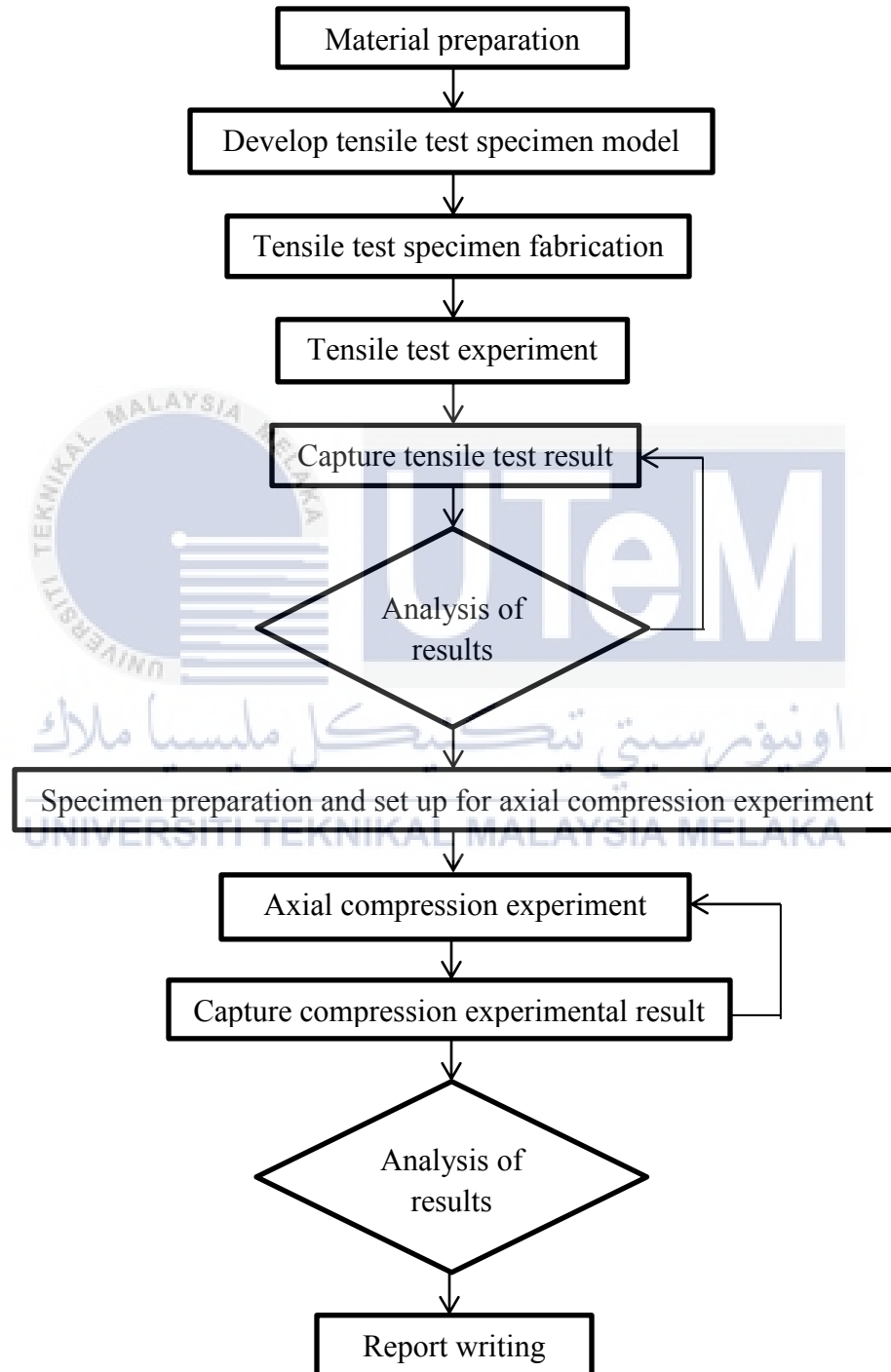


Figure 3.1: Flow chart of the project

In PSM 1, the experiment began with the preparation of materials. The materials such as palm oil saw dust and metal tube was prepared to perform the experiment. For metal tube, one type of circular tube and two type of square tube which made up of aluminium at different dimension. Next, the tensile test was performed in order to obtain the mechanical properties such as Young's Modulus, yield strength and ultimate tensile strength. To perform the tensile test, a tensile test specimen model was designed and developed according to the ASTM standard. The model was drawn by using AutoCAD software. A portion from each type of metal tube was prepared and then fabricated into tensile test specimen by using laser cutting machine. After the specimen was obtained, the tensile test experiment work was carried out by using INSTRON Universal Testing machine. Before the tensile test was carried out, the strain rate of INSTRON Universal Testing machine and the gauge length of specimen were set up. During the tensile test, while the load displacement curve was plotted by the system, the specimen was captured during the specimen yield and after the specimen break. After the tensile test result obtained, the average mechanical properties reading of specimens were calculated. Activities for PSM 1 were tabulated in the Gantt chart as shown in Appendix A1.

In PSM 2, the experiment continued with the axial compression testing. In compression experiment, one type of specimen was prepared into hollow tube and three different density of saw dust filled tube. For each type of aluminium tube, a long metal tube was cut into 8 pieces with specific length using band saw machine. Next, saw dust was inserted into the tube at different compactness and enclosed. Before the specimen was compressed, the mass of hollow and filled tube were weighted by using weight balance. Axial compression experiment was performed using INSTRON quasi-static Universal Testing machine. Load displacement curve was plotted by the system as the experiment started. During axial compression experiment, the deformation behaviour of specimen was captured

and recorded using video camera. After the experiment done, the deform tubes were weighted again and the density is calculated. The experimental result obtained was saved and analysed. Activities for PSM 2 were tabulated in the Gantt chart as shown in Appendix A2.

3.3 Material preparation

The materials used in this experiment work included wood saw dust, circular aluminium tube and square aluminium tube as shown in Figure 3.2.

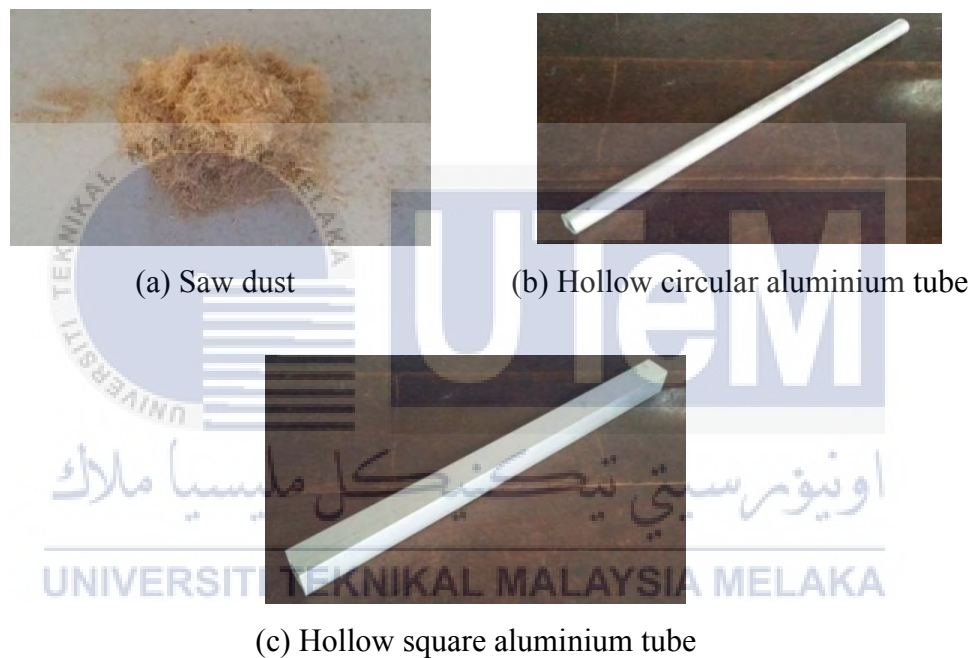


Figure 3.2: Material and specimens used in experiment: (a) Saw dust; (b) Hollow circular aluminium tube; (c) Hollow square aluminium tube

3.3.1 Saw dust

Saw dust used in this experimental work was obtained from the oil palm trunk. Oil palm trunk was milled into smaller size particles and then collected into a plastic bag. Saw dust particle was inserted into the hollow tube before proceed to compressive experimental work.

3.3.2 Hollow aluminium tube

There were three types of hollow aluminium tube shape used in this experiment, with circular tube ($t= 1.50$ mm, $D= 25.3$ mm), square tube ($t= 1.10$ mm, $c= 38.0$ mm) and square tube ($t= 1.10$ mm, $c= 50.6$ mm). The dimension of tube specimen was obtained from measurement using vernier caliper. By using band saw cutting machine, tube specimens were cut into 100 mm for hollow circular aluminium tube and 150 mm for hollow square aluminium tube. Table 3.1 shows the description of hollow aluminium tube dimension used for fabrication.

Table 3.1 Description of materials used

| No | Specimen | Dimension |
|----|--|---|
| 1 |  <p>Hollow circular aluminium tube</p> | <ul style="list-style-type: none"> -Length = 100 mm -Outer diameter = 25.3 mm -Thickness = 1.50 mm |
| 2 |  <p>(i) Hollow square aluminium tube</p> <p>(ii) Hollow square aluminium tube</p> | <ul style="list-style-type: none"> -Length = 150 mm -External Width = 38.0 mm -Thickness = 1.1 mm <ul style="list-style-type: none"> -Length = 150 mm -External Width = 50.6 mm -Thickness = 1.10 mm |

3.4 Preparation of tensile test coupon

A tensile test specimen model was developed using AutoCAD software. To develop tensile test specimen model, American Society for Testing and Materials, ASTM E8 standard reference paper was studied, which covered the tension testing of metallic materials. Based on the ASTM reference, the tensile test specimen was designed according to the specification and dimensions requirement the sheet-type standard specimen as shown in the Figure 3.3.

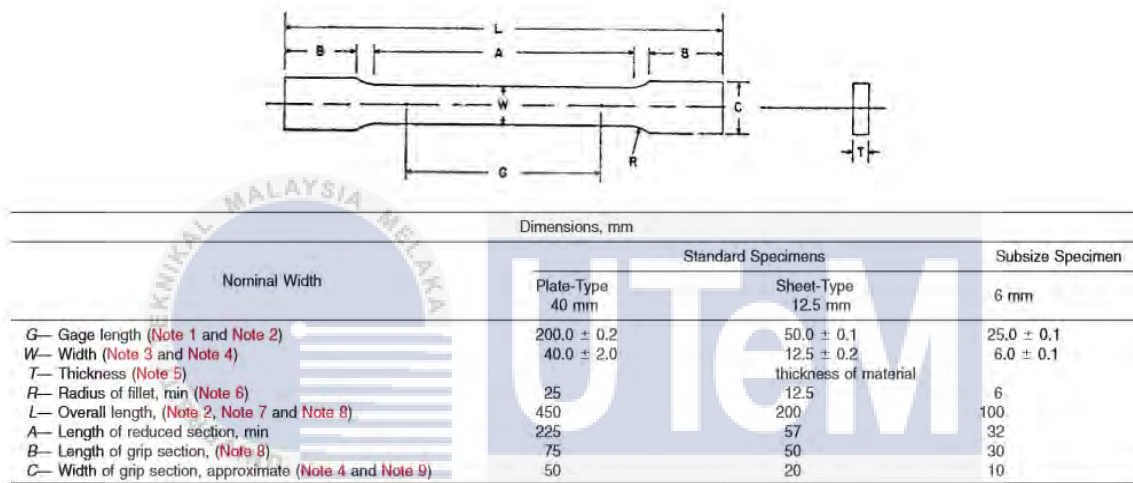


Figure 3.3: Tensile test specimen dimensions from ASTM E8 standard. (ASTM, 2008)

The tensile test specimen drawing was developed using AutoCAD software as shown in Figure 3.4 and Appendix C shows the drawing sheet for tensile test specimen with dimension.

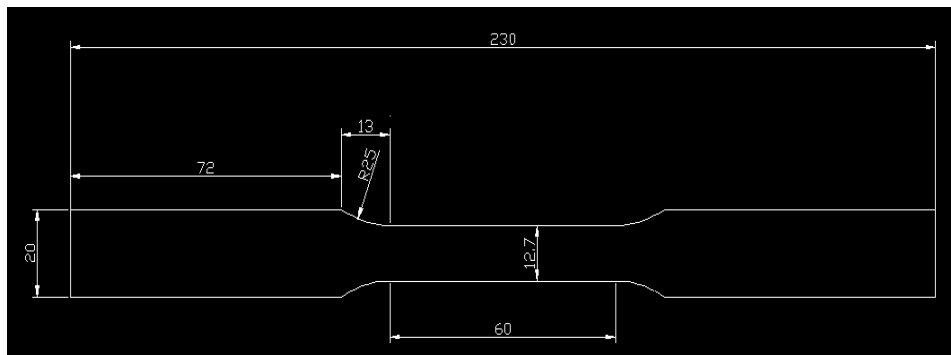


Figure 3.4: Developed tensile test specimen using AutoCAD software

3.5 Tensile test specimen fabrication

After the tensile test specimen drawing was developed using AutoCAD software, laser cutting machine was used to do fabrication. Figure 3.5 shows the laser cutting machine.



Figure 3.5: Laser cutting machine

To perform fabrication work, a suitable laser cutter was firstly chosen according to the type of material. Then, the drawing image was selected that works with the software of laser cutter. After that, the specimen was then inserted with a blocker and gripped. Once the specimen was gripped tightly, laser cutting machine was turned on and waited it warmed up before starting. Next, the laser cutter's line width and its cutting speed was adjusted according to the material while cut out the sheet type specimen. After that, the laser cutting machine was turned off and the sheet type specimen was taken out. Next, the sheet type specimen was left to be cooled down for 10 minutes. Figure 3.6 shows the tensile test specimen after fabrication.



Figure 3.6: Tensile test specimen after fabrication

3.6 Tensile test experiment

The tensile test was conducted by using INSTRON Universal Testing machine. The aim of the performing tensile test was to obtain the mechanical properties which are Young's Modulus, yield strength, ultimate tensile strength and maximum elongation. Figure 3.7 shows the INSTRON Universal Testing Machine used to perform tensile test.



Figure 3.7: INSTRON Universal Testing Machine

To perform the tensile testing of the specimen, the tensile test specimen was firstly to set and marked as shown in the Figure 3.8.

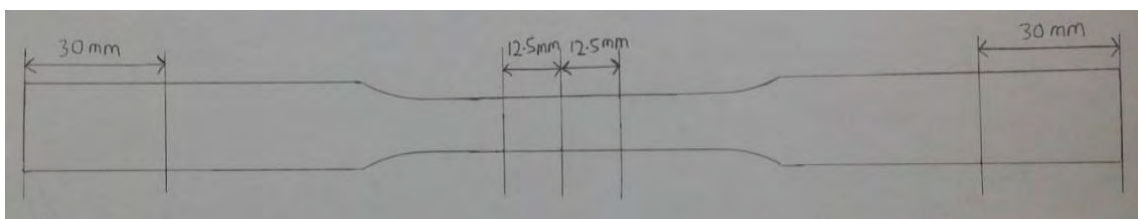


Figure 3.8: Indication marking of tensile test specimen

By using INSTRON Universal Testing machine, the strain rate was set to be 5 mm/min. Experimental testing was carried out on the aluminium sheet type specimens. The gauge length and width of grip section were set to be 25 mm and 20 mm respectively. A gauge length extensometer was used to monitor the specimen strain during testing. The specimen dimension such as width and thickness were measured and the measurements values were inserted into the setup control setting of INSTRON Testing machine. While tensile testing was carried out, INSTRON system recorded the load and strain data digitally throughout the test. Another repeated same aluminium sheet type specimen was then continued with the tensile test. Analysis was done by calculating the average reading of the experimental results.

3.7 Specimen and equipment preparation for axial compression experiment

Before the axial compression experimental work was performed, a series of preparation for specimens needed to be done. Firstly is the preparation for metal tubes. Each type of hollow aluminium tube was cut into 8 pieces using band saw cutting machine. For circular tube ($t= 1.50$ mm, $D= 25.3$ mm), each pieces of aluminium tube was cut into the length of 100 mm, while for square tube ($t= 1.10$ mm, $c= 38.0$ mm) and square tube ($t= 1.10$ mm, $c= 50.6$ mm), each pieces of aluminium tube is cut into length of 150 mm. Figure 3.9 shows the band saw cutting machine used to cut out the aluminium tube into the length requirement.



Figure 3.9: Band saw cutting machine

The procedures to use the band saw cutting machine is as follow.

1. Place the long metal tube on the tilt table of band saw cutting machine.
2. Move the long metal tube against the fixed end of tilt table until it is 90 degree to the cutter.
3. Measure and mark the length of specimen to be cut while adjust the metal tube until the cutter heads to the position of cutting.
4. Lock the metal tube to prevent it moving.
5. Set up the working speed which is suitable to the metal tube.
6. While the cutting operation is carried out, feed the long metal tube with the water at the line of band blade.
7. Lift up the cutter and turn off the feed rate button to remove the tube specimen.

After the aluminium tube cutting, saw dust was then inserted into the tube. Tube filled with saw dust was set up at different density. Three different type of density at ρ_1 , ρ_2 , and ρ_3 was made up by using three different insertion of saw dust amount by portion. The preparation of filled tube to perform experiments at density ρ_1 , ρ_2 , and ρ_3 by using different saw dust insertion by amount is shown in the Table 3.2.

Table 3.2: Preparation of saw dust filled tube at different density

| Density | Ways of saw dust inserted into the tube |
|----------|---|
| ρ_1 | Saw dust was inserted into the tube entirely without compressed |
| ρ_2 | Saw dust was filled about 1/4 of tube length and compressed, and then repeated the steps until saw dust filled into the tube entirely |
| ρ_3 | Saw dust was filled about 1/8 of tube length and compressed, and then repeated the steps until saw dust filled into the tube entirely |

Next, the density of saw dust was calculated. To determine the saw dust density, firstly the masses and inner volumes of tube were determined. Weight balance was used to obtain the mass of the hollow tube and mass of filled tube. Figure 3.10 shows the weight balance to weight the mass of tube.

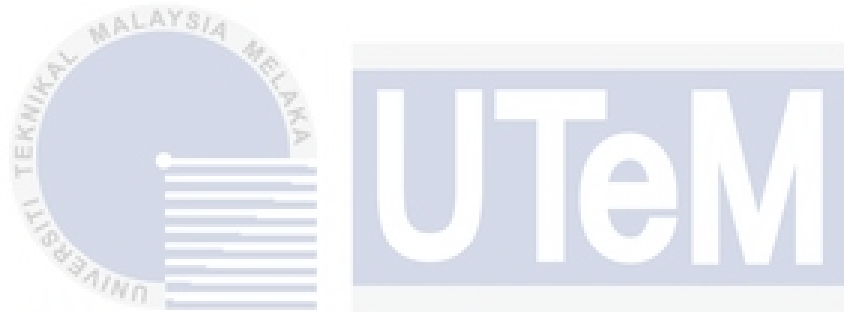


Figure 3.10: Weight balance

To calculate the inner volume of circular and square tube, equation 3.1 and equation 3.2 were used as shown in the below respectively.

$$\text{Inner volume of circular tube} = \left[\pi \times \left(\frac{D_o - 2t}{2} \right)^2 \right] \times \text{Length of tube} \quad (3.1)$$

$$\text{Inner volume of square tube} = (\text{External width} - 2t)^2 \times \text{Length of tube} \quad (3.2)$$



اونيورسيتي تيكنيكل مليسيا ملاك

UNIVERSITI TEKNIKAL MALAYSIA MELAKA

Before the experimental work started, the INSTRON Universal Testing machine was set up from the system. The strain rate was set to be 10 mm/min. All of the experiment test will be performed at the room temperature. Hollow aluminium tube was firstly run the compression test, followed by saw dust filled tube at three different densities for same type of specimen. The compression test experiment was then repeated with another type of aluminium tube using same method.

The procedure to use the INSTRON 5585 Universal Testing machine is as follow.

1. Open Bluehill and select the set up button to adjust and program the control setting.
2. Determine the parameters and the end result to be obtained.
3. Key in also the dimension of the specimen.
4. Install the specimen to the machine and tighten it up.
5. Click the Bluehill Test button.
6. Click the balance all button to set all the load and displacement to become zero.
7. Start the test by click on the start button.

3.9 Capturing experimental result

A video camera was used to capture and record the deformation pattern of aluminium tube specimens during quasi-static compression experiment. Figure 3.12 shows the video camera used to capture the tube deformation pattern.



Figure 3.12: Video camera

Tripod and LED emitting light were used throughout the experiment. Tripod was used to hold the video camera so that video camera can instantly capture the specimen deforming behavior. While capturing during the experiment, LED emitting light was placed besides the specimen to enable the video camera for clear vision through the specimen. The deformation pattern for each type of specimen was recorded and observed.

CHAPTER 4

RESULTS AND DISCUSSION

4.1 Description

The experiment of empty and saw dust filled tube under axial compression was conducted by using INSTRON quasi-static Universal Testing Machine. The test specimen used was aluminium made of circular and square tube which compressed at the rate of 10 mm/min. Load displacement curve was obtained during the experiment. The experimental results were summarised in term of density, deforming mode, theoretical and experimental mean load, plastic wavelength, energy absorbed and specific energy. Experimental result was analysed at different specimen size and saw dust density.

4.2 Density of Saw Dust

Saw dust was inserted into the tube with different compactness. The compactness of saw dust was divided into four different densities, ρ_0 , ρ_1 , ρ_2 and ρ_3 made at different methods. For density ρ_0 , tube specimens did not inserted with saw dust, the density was 0. For density ρ_1 , saw dust was filled into the tube without compressed. The compactness of the saw dust depends on the gravitational acceleration. For density ρ_2 , saw dust was filled until 1/4 of the tube length and compressed. Next, saw dust was filled into another 1/4 again of same tube then compressed and the insertion of saw dust was repeated until it filled fully. For density ρ_3 , saw dust was filled until 1/8 of the tube length and compressed. Saw dust was filled into another 1/8 again of same tube then compressed and the insertion of saw dust was repeated

until it filled fully.

After the insertion of saw dust, all the specimens of hollow and filled tube were weighed by using weight balance to determine the weight of saw dust inside the tube. The weight of each type specimen had been recorded and tabulated.

The inner volume of hollow circular and square tube was calculated as follow:

(i) For circular tube:

Length, $L = 100$ mm, Thickness, $t = 1.50$ mm, Outer diameter, $D = 25.3$ mm

$$\text{Inner volume of circular tube} = \left[\pi \times \left(\frac{d_o - 2t}{2} \right)^2 \right] \times \text{Length of tube}$$

$$= \left[\pi \times \left(\frac{0.0253 - 2(0.0015)}{2} \right)^2 \right] \times 0.1$$
$$= 3.9057 \times 10^{-5} \text{ m}^3$$

(ii) For square tube:

Length, $L = 150$ mm, Thickness, $t = 1.10$ mm, External width, $c = 38.0$ mm

$$\text{Inner volume of square tube} = (\text{External width} - 2t)^2 \times \text{Length of tube}$$

$$= [0.038 - 2(0.0011)]^2 \times 0.15$$
$$= 1.9225 \times 10^{-4} \text{ m}^3$$

(iii) For square tube:

Length, $L = 150$ mm, Thickness, $t = 1.10$ mm, External width, $c = 50.6$ mm

$$\text{Inner volume of square tube} = (\text{External width} - 2t)^2 \times \text{Length of tube}$$

$$= [0.0506 - 2(0.0011)]^2 \times 0.15$$
$$= 3.5138 \times 10^{-4} \text{ m}^3$$

Table 4.1, Table 4.2 and Table 4.3 show the calculation result of saw dust density of circular and two different dimension of square tube at different ways of insertion.

Table 4.1: Calculation of saw dust density of circular tube (Length, L = 100 mm, Thickness, t = 1.50 mm, Outer diameter, D = 25.3 mm)

| Circular Tube | Density = ρ_0 (Empty Tube) | | Density = ρ_1 (Sawdust filled without compressed) | | Density = ρ_2 (Sawdust filled about 1/4 of tube length and compressed and repeated until it filled fully) | | Density = ρ_3 (Sawdust filled about 1/8 of tube length and compressed and repeated until it filled fully) | |
|---|------------------------------------|------|---|------------------------|--|------------------------|--|------------------------|
| | 1 | 2 | 1 | 2 | 1 | 2 | 1 | 2 |
| Mass of empty tube (g) | 29.8 | 29.9 | 30.0 | 29.9 | 29.9 | 29.9 | 29.9 | 30.0 |
| Mass of sawdust filled tube before compressed (g) | 29.8 | 29.9 | 38.6 | 38.9 | 41.5 | 41.5 | 42.3 | 42.6 |
| Density before compressed (kg/m^3) | 0 | 0 | 220.19 | 230.43 | 297.00 | 297.00 | 317.48 | 322.61 |
| Mass of saw dust filled tube after compressed (g) | - | - | 34.9 | 34.4 | 35.1 | 34.7 | 34.6 | 35.2 |
| Length of filled tube after compressed (mm) | - | - | 25.69 | 23.33 | 26.26 | 26.52 | 26.78 | 29.73 |
| Volume of filled tube after compressed (m^3) | - | - | 1.003×10^{-5} | 9.112×10^{-6} | 1.026×10^{-5} | 1.036×10^{-5} | 1.046×10^{-5} | 1.161×10^{-5} |
| Density after compressed (kg/m^3) | - | - | 3.480×10^3 | 3.775×10^3 | 3.421×10^3 | 3.349×10^3 | 3.308×10^3 | 3.032×10^3 |

Table 4.2: Calculation of saw dust density of square tube (Length, L = 150 mm, Thickness, t = 1.10 mm, External width, c = 38.0 mm)

| Square Tube | Density = ρ_0 (Empty Tube) | | Density = ρ_1 (Sawdust filled without compressed) | | Density = ρ_2 (Sawdust filled about 1/4 of tube length and compressed and repeated until it filled fully) | | Density = ρ_3 (Sawdust filled about 1/8 of tube length and compressed and repeated until it filled fully) | |
|---|------------------------------------|------|---|------------------------|--|------------------------|--|------------------------|
| | 1 | 2 | 1 | 2 | 1 | 2 | 1 | 2 |
| Mass of empty tube (g) | 64.5 | 63.8 | 61.4 | 62.8 | 62.5 | 61.5 | 63.4 | 62.8 |
| Mass of sawdust filled tube before compressed (g) | 64.5 | 63.8 | 94.6 | 96.6 | 114.8 | 125.3 | 130.7 | 135.3 |
| Density before compressed (kg/m^3) | 0 | 0 | 172.69 | 175.81 | 272.04 | 331.86 | 350.07 | 377.11 |
| Mass of saw dust filled tube after compressed (g) | - | - | 92.7 | 95.2 | 113.8 | 124.5 | 129.4 | 134.4 |
| Length of filled tube after compressed (mm) | - | - | 28.75 | 30.25 | 37.53 | 34.54 | 42.92 | 43.46 |
| Volume of filled tube after compressed (m^3) | - | - | 3.685×10^{-5} | 3.877×10^{-5} | 4.810×10^{-5} | 4.427×10^{-5} | 5.501×10^{-5} | 5.570×10^{-5} |
| Density after compressed (kg/m^3) | - | - | 2516 | 2456 | 2366 | 2812 | 2352 | 2413 |

Table 4.3: Calculation of saw dust density of square tube (Length, L = 150 mm, Thickness, t = 1.10 mm, External width, c = 50.6 mm)

| Square Tube | Density = ρ_0 (Empty Tube) | | Density = ρ_1 (Sawdust filled without compressed) | | Density = ρ_2 (Sawdust filled about 1/4 of tube length and compressed and repeated until it filled fully) | | Density = ρ_3 (Sawdust filled about 1/8 of tube length and compressed and repeated until it filled fully) | |
|---|------------------------------------|------|---|------------------------|--|------------------------|--|------------------------|
| | 1 | 2 | 1 | 2 | 1 | 2 | 1 | 2 |
| Mass of empty tube (g) | 79.3 | 78.6 | 79.6 | 79.6 | 79.4 | 78.9 | 79.7 | 79.4 |
| Mass of sawdust filled tube before compressed (g) | 79.3 | 78.6 | 137.0 | 138.4 | 167.2 | 173.3 | 189.6 | 201.6 |
| Density before compressed (kg/m^3) | 0 | 0 | 163.36 | 167.34 | 249.87 | 268.66 | 312.77 | 347.77 |
| Mass of saw dust filled tube after compressed (g) | - | - | 132.3 | 136.9 | 161.4 | 168.4 | 183.2 | 195.7 |
| Length of filled tube after compressed (mm) | - | - | 36.34 | 37.14 | 35.63 | 34.92 | 35.28 | 37.25 |
| Volume of filled tube after compressed (m^3) | - | - | 8.513×10^{-5} | 8.700×10^{-5} | 8.347×10^{-5} | 8.180×10^{-5} | 8.265×10^{-5} | 8.726×10^{-5} |
| Density after compressed (kg/m^3) | - | - | 1954 | 1974 | 1934 | 2059 | 2217 | 2243 |

4.3 Deformation characteristics

4.3.1 Circular tube deformation

For circular tube ($L = 100$ mm, $t = 1.5$ mm, $D = 25.3$ mm), tube deformed in multi lobe mode. The deformation mode of circular tube is influenced by ratio of diameter to thickness (D/t), ratio of length to diameter (L/D) and material properties.

Figure 4.1 shows progressive axial crushing of circular tube ($L = 100$ mm, $t = 1.50$ mm, $D = 25.3$ mm). The deformation behavior of circular tube in the first 5 mm of compressive displacement formed a circumferential plastic hinge at the end of tube, followed by folding into two lobes at opposite to each other in 10 mm compressive deformation. Elliptical plastic hinge formed at both end of the lobe. In 10 mm compressive displacement, the first plastic fold was completed which brought towards the second fold beginning at 15 mm compressive displacement. During the interval from 10 mm to 15 mm, tube deformed laterally after forming the first fold. Second fold began to develop after the lateral deformation from 20 mm until 40 mm compressive displacement. During the interval from 40 mm to 45 mm compressive displacement, tube deformed laterally again after forming the second fold. Plastic folding continued to develop began from 50 mm until 65 mm compressive displacement for third fold. Progressive loading keep resume until no longer plastic folding occurred at 80 mm displacement.

Circular Tube (Length, $L= 100$ mm, Thickness, $t= 1.50$ mm, Outer diameter, $D= 25.3$ mm)



Figure 4.1: Progressive axial crushing of circular tube ($L= 100$ mm, $t= 1.50$ mm, $D= 25.3$ mm)

Figure 4.2 shows some deformation pattern of circular tube ($L = 100$ mm, $t = 1.5$ mm, $D = 25.3$ mm) in axial compression experiment. Some indications were made. Firstly, circular tube ($L = 100$ mm, $t = 1.5$ mm, $D = 25.3$ mm) formed circumference plastic hinge as at the end of tube once it compressed. Secondly, circular tube formed multi lobes fold as it compressed further. Thirdly, each layer of fold formed elliptical plastic hinge for each lobe produced.

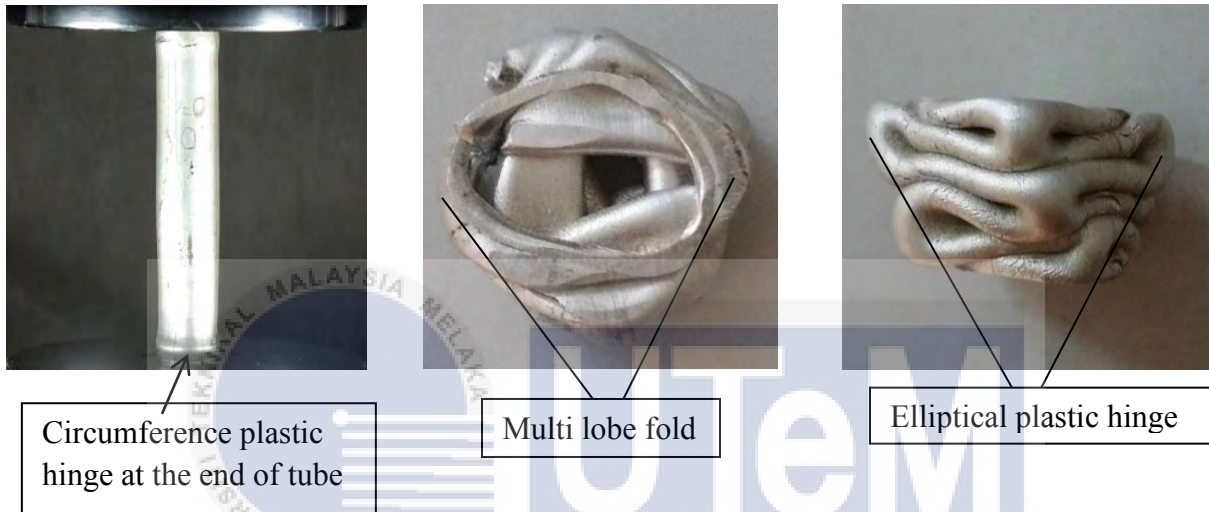


Figure 4.2: Deformation pattern of circular tube ($L = 100$ mm, $t = 1.5$ mm, $D = 25.3$ mm)

For filled circular tube ($L=100$ mm, $t=1.5$ mm, $D=25.3$ mm), saw dust does not alter the deforming mode of circular tube at different density (remain as multi lobe mode). Appendix 2 shows the progressive crushing of saw dust filled circular tube at different density.

4.3.2 Square tube deformation

For square tube ($L = 150$ mm, $t = 1.1$ mm, $c = 38.0$ mm), tube deformed in diamond mode with severe inward and outward plastic bending. Progressive collapse caused tube formed plastic hinge, plastic bending and plastic folding. As tube was further compressed, one by one plastic folding layer was produced until compact collapse mode was formed. Figure 4.3

shows deformation pattern of square tube ($L = 150 \text{ mm}$, $t = 1.1 \text{ mm}$, $c = 38.0 \text{ mm}$).

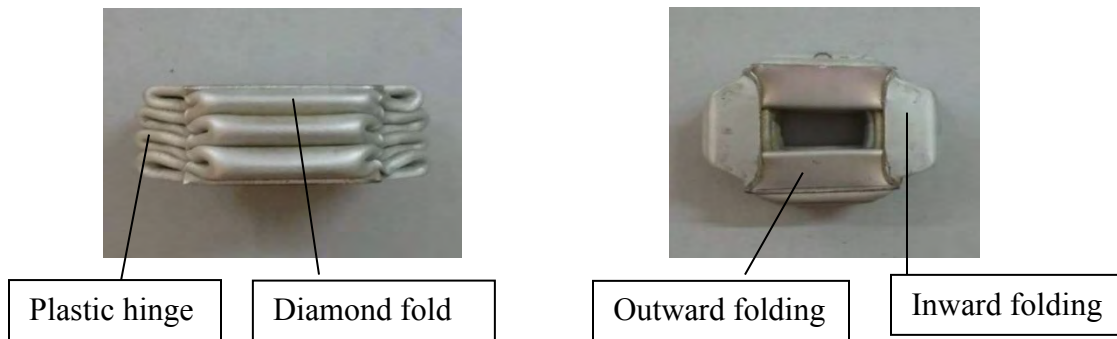


Figure 4.3: Deformation pattern of square tube ($L = 150 \text{ mm}$, $t = 1.1 \text{ mm}$, $c = 38.0 \text{ mm}$)

Figure 4.4 shows the progressive axial crushing behaviour of square tube ($L=150 \text{ mm}$, $t = 1.10 \text{ mm}$, $c = 38.0 \text{ mm}$). In first 2 mm of compressive displacement, tube began to form inward and outward folds. From 10 mm to 20 mm compressive displacement, first fold was accomplished by progressive collapse to complete inward and outward plastic fold. Horizontal and inclined hinge produced during the formation of first fold. In 20 mm of compressive displacement, fold layer came into contact indicated the completion of first fold. Progressive compression of tube proceed with initiation of bending line for second inward and outward fold in the 30 mm compressive displacement. Starting from 40 mm compressive displacement, axial compression brought the tube towards the formation of second plastic fold and the fold completed in 60 mm compressive displacement. Plastic bending line was formed after the completion of second plastic fold. Beginning from 70 mm compressive displacement, third inward and outward plastic fold was formed by circular tube until it completed in 90 mm compressive displacement. Another plastic bending line was formed once the completion of third fold. In 95 mm compressive displacement, plastic folding continued to form after the third fold. The progressive folding accomplished until 120 mm compressive displacement to form complete compact diamond mode.

Square Tube (Length = 150 mm, Thickness, $t = 1.10$ mm, External width, $c = 38.0$ mm)

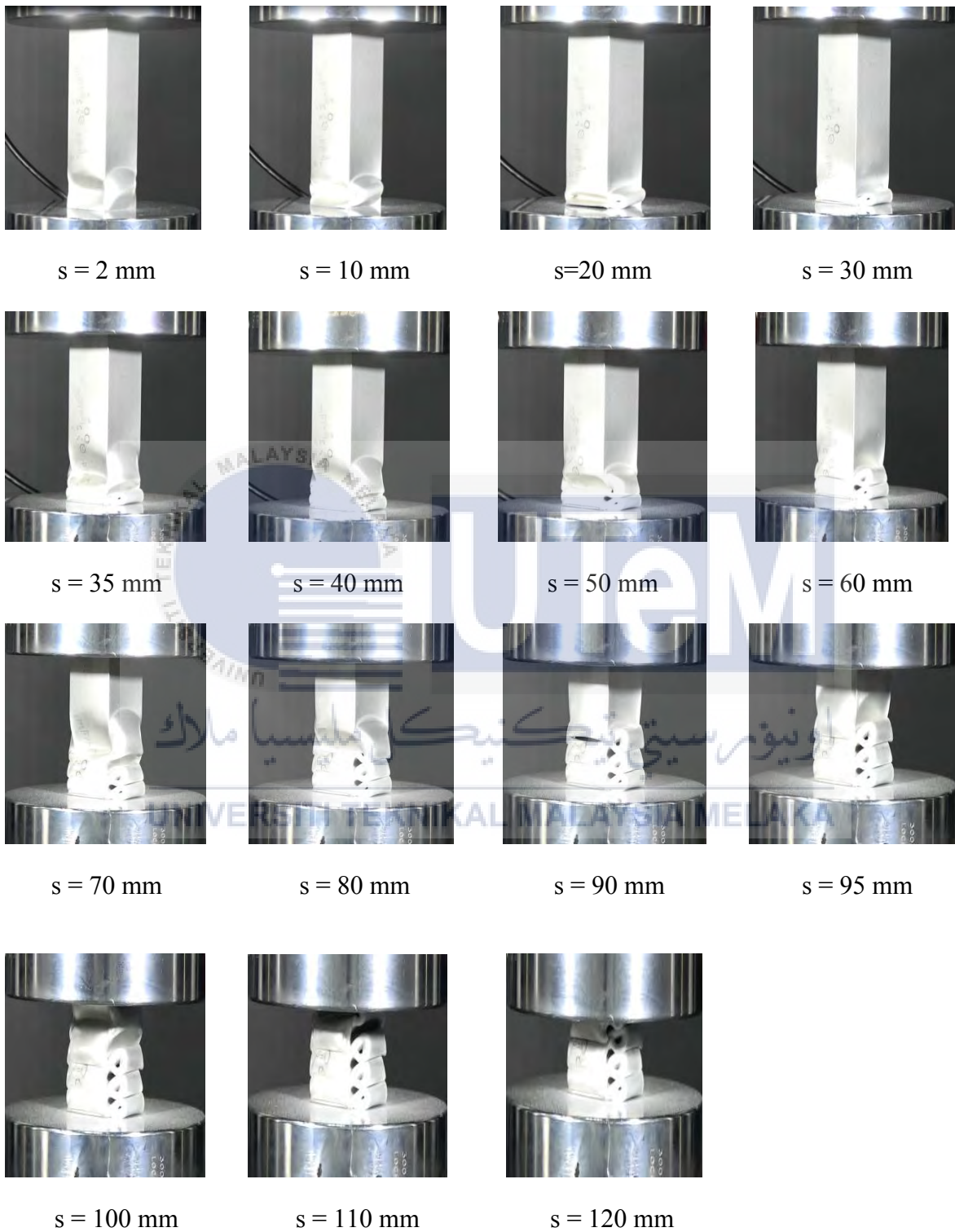


Figure 4.4: Progressive axial crushing behaviour of square tube ($L=150$ mm, $t = 1.10$ mm, $c = 38.0$ mm)

For square tube ($L = 150 \text{ mm}$, $t = 1.1 \text{ mm}$, $c = 50.6 \text{ mm}$), tube deformed in diamond mode, with inward and outward fold. Axial compression loading caused square tube undergoes plastic folding with non-compact mode. Non-compact collapse mode is the deformation mode where the folds are not continuous and the folds are separated by slightly curved panels. Figure 4.5 shows the deformation pattern of square tube ($L = 150 \text{ mm}$, $t = 1.1 \text{ mm}$, $c = 50.6 \text{ mm}$).

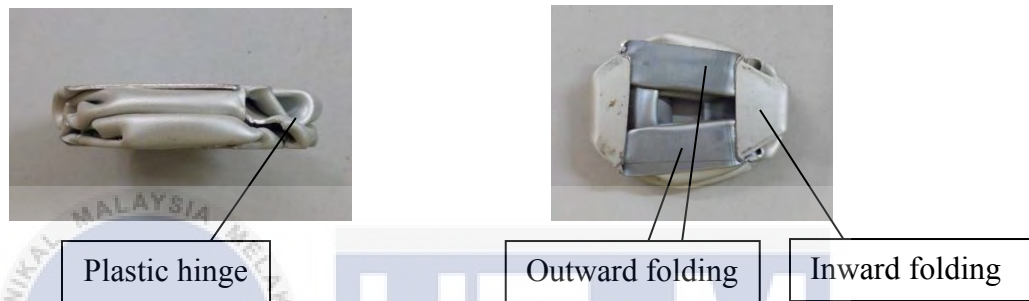


Figure 4.5: Deformation pattern of square tube ($L = 150 \text{ mm}$, $t = 1.1 \text{ mm}$, $c = 50.6 \text{ mm}$)

Figure 4.6 shows the progressive axial crushing behavior of square tube ($L = 150 \text{ mm}$, $t = 1.10 \text{ mm}$, $c = 50.6 \text{ mm}$). In the first 2 mm compressive displacement, square tube ($L = 150 \text{ mm}$, $t = 1.1 \text{ mm}$, $c = 50.6 \text{ mm}$) started to produce inward and outward fold. Progressive collapse to form first plastic fold was accomplished until 30 mm compressive displacement. Plastic hinge was produced after the formation of first fold. In 30 mm compressive displacement, square tube deformed inwards laterally. Progressive compression continued to form plastic bending line to form another plastic fold. Starting from 40 mm compressive displacement, axial compression brought the tube towards the formation of second plastic fold and the fold completed in 70 mm compressive displacement. In 70 mm compressive displacement, another inward and outward bending line was formed, which initiated into another folding. Starting from 70 mm compressive displacement, third fold accomplished until 120 mm compressive displacement to form complete non compact diamond mode.

Square Tube (Length = 150 mm, Thickness, $t = 1.10$ mm, External width, $c = 50.6$ mm)

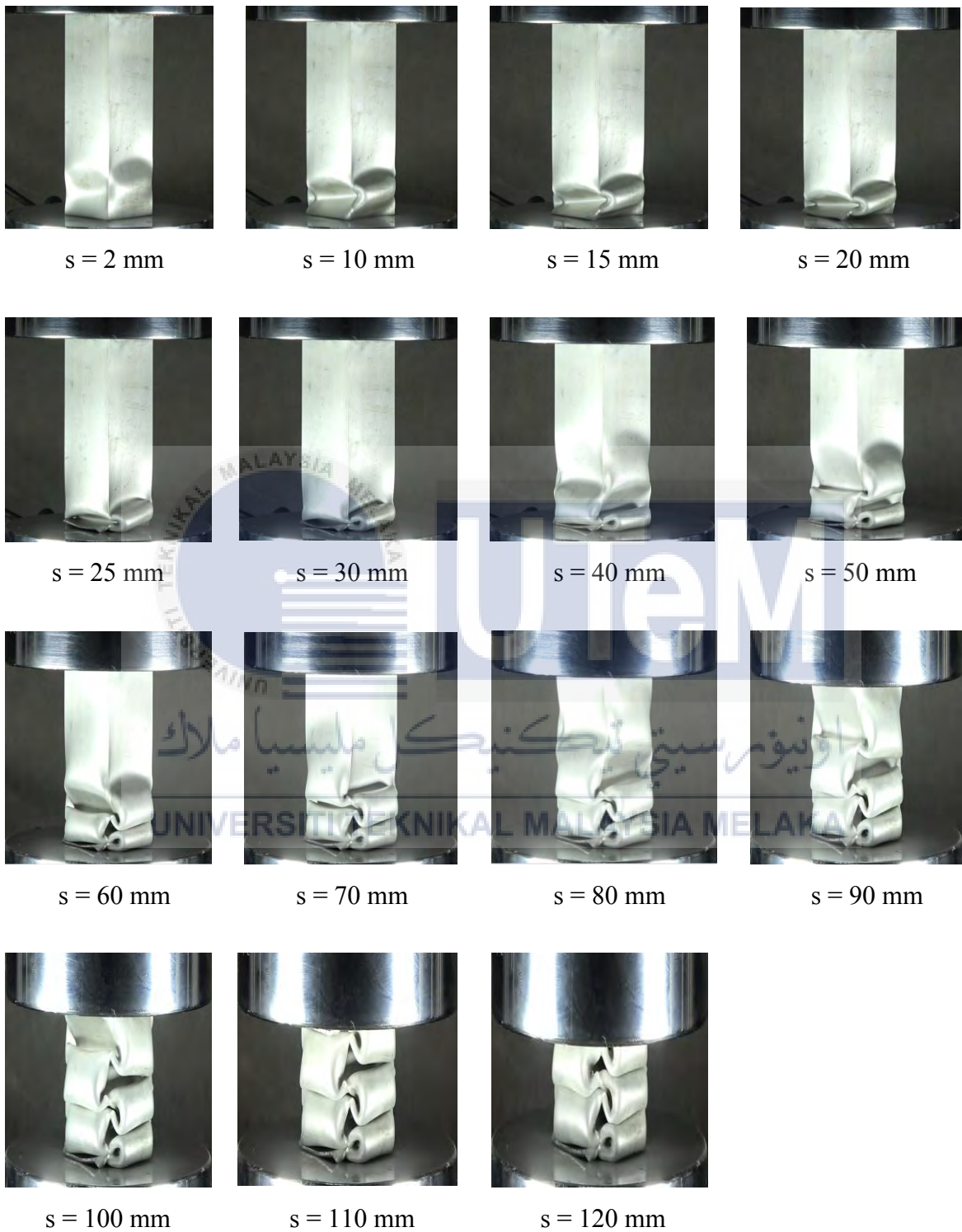


Figure 4.6: Progressive axial crushing behaviour of square tube ($L=150$ mm, $t = 1.10$ mm, $c = 50.6$ mm)

4.3.3 Saw dust filled tube deformation

Appendix B1, B2 and B3 show the progressive crushing of selected density of saw dust filled circular tube ($L=100$ mm, $t=1.5$ mm, $D=25.3$ mm), square tube ($L=150$ mm, $t= 1.10$ mm, $c= 38.0$ mm) and square tube ($L=150$ mm, $t= 1.10$ mm, $c= 50.6$ mm) respectively. For filled circular tube ($L=100$ mm, $t=1.5$ mm, $D=25.3$ mm), saw dust does not alter the deforming mode of circular tube at different density (remain as multi lobe mode). Same as the filled square tube ($L=150$ mm, $t= 1.10$ mm, $c= 38.0$ mm), saw dust does not change the deforming mode of square at different density. Both circular tube ($L=100$ mm, $t=1.5$ mm, $D=25.3$ mm) and square tube ($L=150$ mm, $t= 1.10$ mm, $c= 38.0$ mm) decreased in overall length shortening when the initial saw dust density increase. For square tube ($L=150$ mm, $t= 1.10$ mm, $c= 50.6$ mm), the presence of saw dust does not show deforming mode characteristics, but causes the tube specimen to break and split beginning at the corner of square tube. Figure 4.7 shows the breaking behaviour of square tube ($L=150$ mm, $t= 1.10$ mm, $c= 50.6$ mm) during quasi-static axial loading.



Figure 4.7: Breaking behaviour of square tube ($L=150$ mm, $t= 1.10$ mm, $c= 50.6$ mm) during quasi-static axial loading

4.4 Tensile test result

One of the mechanical properties of result such as Modulus of elasticity, yield strength, tensile strength and maximum deformation from selected tensile test sample are obtained as shown in the Appendix D. During the tensile test, stress strain curve was plotted by the INSTRON system during tensile testing. Figure 4.8 shows one of stress against strain curve obtained from a tensile test experiment.

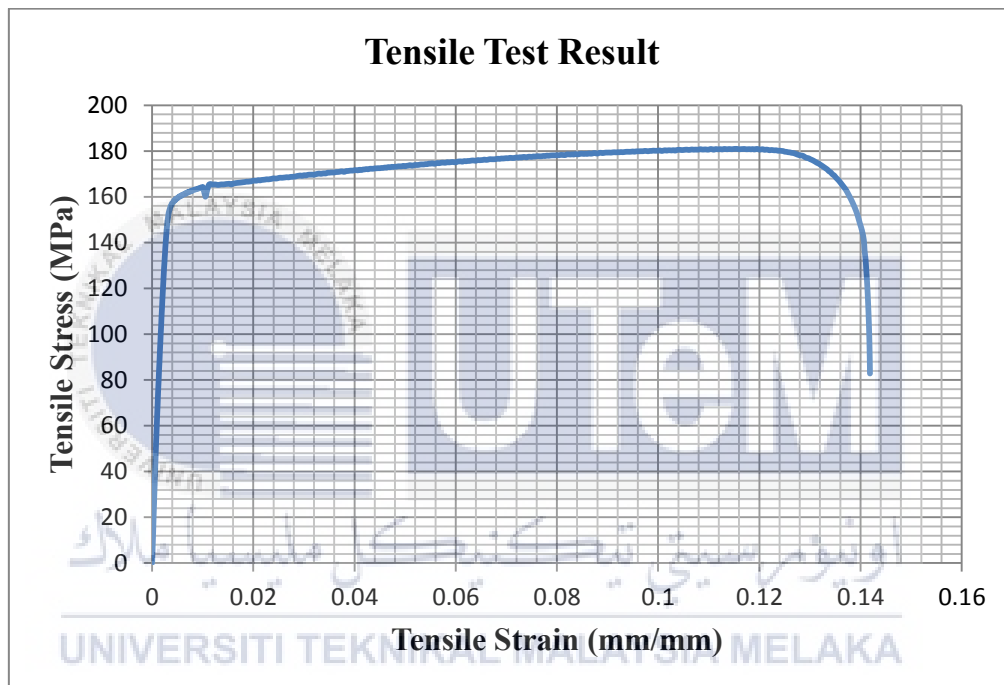


Figure 4.8: Stress against strain curve from tensile test experiment

Table 4.4 shows the tensile testing results of four tensile test specimen made of aluminium.

Table 4.4: Tensile testing result of aluminium tensile test specimen

| Mechanical Properties | Specimen Sample | | | | Average |
|------------------------------------|-----------------|---------|---------|---------|---------|
| | 1 | 2 | 3 | 4 | |
| Modulus of elasticity (GPa) | 67.270 | 69.121 | 59.907 | 59.855 | 64.038 |
| Yield strength (Offset 0.2%) (MPa) | 145.699 | 159.354 | 150.511 | 157.207 | 153.193 |
| Ultimate tensile strength (MPa) | 176.546 | 180.958 | 172.853 | 179.134 | 177.373 |
| Maximum deformation (mm) | 5.894 | 3.520 | 3.934 | 4.072 | 4.355 |

4.5 Comparison of experimental results with theory

4.5.1 Theoretical calculation of plastic wavelength and mean load

Hollow circular tube

From theoretical studies conducted by Singace, the mean crushing load of hollow circular tube deformed in multi-lobe mode is given by equation 4.1 and 4.2.

$$P_m = M_o \left(-\frac{\pi}{3}N + \frac{2\pi^2}{N} \tan \left(\frac{\pi}{2N} \right) \frac{D}{t} \right) \quad (4.1)$$

$$P_m = \frac{\sigma_{ys} t^2}{2\sqrt{3}} \left(-\frac{\pi}{3}N + \frac{2\pi^2}{N} \tan \left(\frac{\pi}{2N} \right) \frac{D}{t} \right) \quad (4.2)$$

The average yield stress is 153.19 MPa obtained from the series of tensile test result.

Hollow circular tube deformed into two lobes per circumference, therefore

$$P_m = \frac{(153.19 \times 10^6)(0.0015)^2}{2\sqrt{3}} \left[-\frac{\pi}{3}(2) + \frac{2\pi^2}{2} \tan \left(\frac{\pi}{2(2)} \right) \frac{0.0253}{0.0015} \right]$$
$$= 16.355 \text{ kN}$$

To calculate the plastic wavelength of hollow circular tube, the equation for half plastic wavelength, H_m is given by equation 4.3.

$$H_m = 0.95\sqrt{Dt} \quad (4.3)$$

The half plastic wavelength of circular tube is

$$H_m = 0.95\sqrt{(0.0253)(0.0015)}$$
$$= 5.85 \text{ mm}$$

Therefore, for one complete plastic wavelength is $2H_m = 11.70 \text{ mm}$

Saw dust filled circular tube

To determine the mean crushing load of own saw dust, using equation 4.4.

$$P_w = \frac{\pi}{4} D^2 \sigma_w \quad (4.4)$$

where σ_w is given by

$$\sigma_w = A \sigma_{ws} \exp^{0.5\left(\frac{\rho}{\rho_s} - B\right)} \quad (4.5)$$

where $A = 0.93$, $B = 0.723$ are saw dust grade constant

The mean crushing load of wood-filled tubes deforming into the multi-lobe mode is given by equation 4.6.

$$P_m^w = P_m + P_w \quad (4.6)$$

Sample calculation

For saw dust density at $\rho = 220.19 \text{ kg/m}^3$ and $\rho_s = 3480 \text{ kg/m}^3$

$$\begin{aligned} \sigma_w &= 0.93(4 \times 10^6) \exp^{0.5\left(\frac{220.19}{3480} - 0.723\right)} \\ &= 2.675 \text{ MPa} \end{aligned}$$

$$P_w = \frac{\pi}{4} (0.0253)^2 (2.675 \times 10^6)$$

$$= 1.345 \text{ kN}$$

The mean crushing load of wood-filled tubes deforming into the multi-lobe mode is given by

$$P_m^w = P_m + P_w$$

$$= 16.355 + 1.345$$

$$= 17.70 \text{ kN}$$

Hollow square tube

The mean load, P_m and the half plastic wavelength, H_m of empty square tube are shown in the equation 4.7 and equation 4.8 respectively.

$$P_m = 9.56Y \sqrt[3]{ct^5} \quad (4.7)$$

$$H_m = 0.983 \sqrt[3]{c^2t} \quad (4.8)$$

Sample calculation

The mean load, P_m and the half plastic wavelength, H_m for hollow square tube ($L = 150$ mm, $t = 1.1$ mm, $c = 38.0$ mm) was

$$P_m = 9.56(177.37 \times 10^6) \left(\sqrt[3]{(0.038)(0.0011)^5} \right) \\ = 6.682 \text{ kN}$$

$$H_m = 0.983 \sqrt[3]{(0.038)^2(0.0011)} \\ = 11.47 \text{ mm}$$

One complete plastic wavelength, $2H_m = 22.94$ mm

On the other hand, the theoretical calculation of mean load and the plastic wavelength for square tube ($L = 150$ mm, $t = 1.1$ mm, $c = 50.6$ mm) was

$$P_m = 9.56(177.37 \times 10^6) \left(\sqrt[3]{(0.0506)(0.0011)^5} \right) \\ = 7.352 \text{ kN}$$

$$H_m = 0.983 \sqrt[3]{(0.0506)^2(0.0011)} \\ = 13.88 \text{ mm}$$

One complete plastic wavelength is $2H_m = 27.76$ mm

Saw dust filled square tube

The mean crushing load of saw dust itself is determined from equation 4.9.

$$P_w = \text{Area} \times \sigma_w \quad (4.9)$$

where σ_w is given from equation 4.5.

The mean crushing load of wood-filled tubes deforming into the multi-lobe mode is determined from equation 4.6.

Sample calculation

For saw dust density at $\rho = 172.69 \text{ kg/m}^3$ and $\rho_s = 3480 \text{ kg/m}^3$

$$\sigma_w = 0.93(4 \times 10^6) \exp^{0.5\left(\frac{172.69}{3480} - 0.723\right)}$$

$$= 2.657 \text{ MPa}$$

$$P_w = (0.038)^2(2.657 \times 10^6)$$

$$= 3.836 \text{ kN}$$

The mean crushing load of wood-filled tubes deforming into the multi-lobe mode is given by

$$P_m^w = 6.682 + 3.836$$

$$= 10.518 \text{ kN}$$

4.5.2 Experimental results and of plastic wavelength and mean load

The experimental result of plastic wavelength and the mean load for circular and square tubes were obtained by using statistical function of Excel. Data sources obtained from experiment was excessed in Excel to plot the load displacement curve. The mean load and plastic wavelength are estimated from the curve and then compare with the theory. To determine the experimental mean load, the entire load obtained from data source was summing up and divided by total number of frequency data. On the other hand, plastic wavelength is determined from the successive peak load in the load displacement curve. The determination for experimental plastic wavelength and mean load are illustrated as shown in the Figure 4.9.

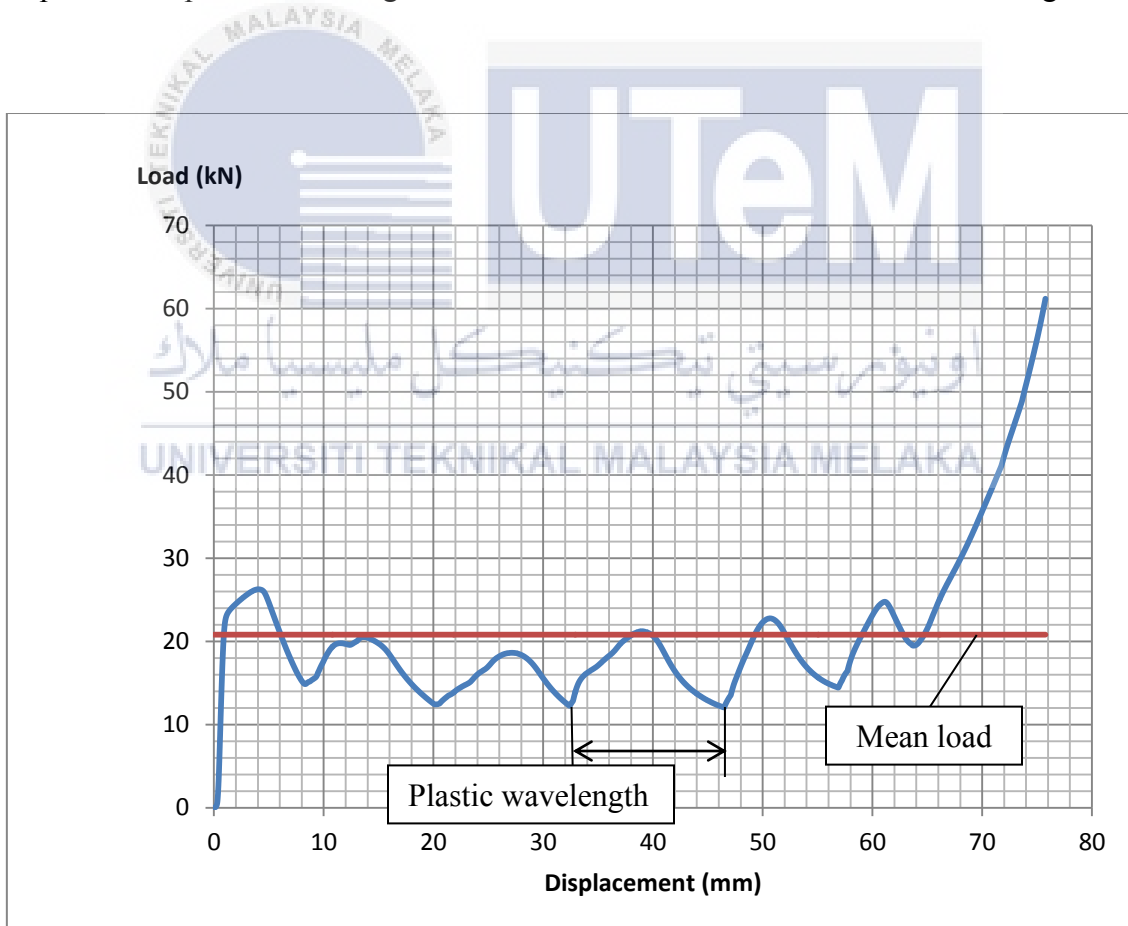


Figure 4.9: Illustration of determine mean load and plastic wavelength of circular tube ($L = 100$ mm, $t = 1.5$ mm, $D = 25.3$ mm)

4.5.3 Comparison of mean load

Table 4.5 shows the comparison for theoretical and experimental result of mean load for hollow circular and both type of squares tube.

Table 4.5: Theoretical and experimental mean crushing load of hollow tube

| Specimen | P_{mean} (kN) | P_{exp} (kN) | % difference |
|----------------------|------------------------|-----------------------|--------------|
| Circular (25.3 mm) 1 | 16.355 | 14.878 | 9.03 |
| Circular (25.3 mm) 2 | 16.355 | 15.227 | 6.70 |
| Square (38 mm) 1 | 6.682 | 8.103 | 21.27 |
| Square (38 mm) 2 | 6.682 | 7.653 | 14.53 |
| Square (50.6 mm) 1 | 7.352 | 7.754 | 5.47 |
| Square (50.6 mm) 2 | 7.352 | 7.778 | 5.79 |

The mean crushing load for circular tube ($L = 100$ mm, $t = 1.5$ mm, $D = 25.3$ mm) was the highest, with 16.355 kN calculated from theoretical equation while 14.878 kN and 15.427 kN obtained from the experimental results. However, square tube ($L = 150$ mm, $t = 1.1$ mm, $c = 38.0$ mm) had the lowest mean crushing load, with 6.682 kN calculated from equation while 8.103 kN and 7.653 kN obtained from experimental result. The higher mean crushing load of circular tube was mainly caused by higher thickness of with 1.5 mm as compare to square tube with thickness 1.1 mm. Therefore, higher axial compression load required to produce plastic collapse. On the other hand, the mean crushing load for square tube ($L = 150$ mm, $t = 1.1$ mm, $c = 50.6$ mm) was 7.352 kN from theoretical calculation while 7.754 kN and 7.778 kN from the experimental result.

Square tube ($L = 150$ mm, $t = 1.1$ mm, $c = 50.6$ mm) has higher theoretical mean load than the square tube ($L = 150$ mm, $t = 1.1$ mm, $c = 38.0$ mm). The different of the mean load are caused by different in side length, c . A bigger side length square tube would have the higher total surface area. Therefore, higher axial compression load is required to produce deformation and also plastic collapse. By comparison between the experimental result with

theory, the percentage difference was higher for square tube ($L = 150$ mm, $t = 1.1$ mm, $c = 38.0$ mm). The higher percentage difference was caused by the uneven plastic folding during the quasi static loading.

For filled tube, the presence of saw dust in tube alters the amount of load to deform at different density. Saw dust has the effect to enhance the stability of tube and delay the plastic collapse. Table 4.6 shows the theoretical and experimental mean crushing load of saw dust filled tube.

Table 4.6: Theoretical and experimental mean crushing load of saw dust filled tube

| | Density before compressed (kg/m^3) | Density after compressed (kg/m^3) | P_{mean} (kN) | P_{exp} (kN) | % difference |
|---|---|--|------------------------|-----------------------|--------------|
| Circular Tube ($L = 100$ mm, $t = 1.5$ mm, $D = 25.3$ mm) | | | | | |
| ρ_1 | 220.19 | 3480 | 17.70 | 16.481 | 6.89 |
| | 230.43 | 3775 | 17.698 | 16.579 | 6.32 |
| ρ_2 | 297.00 | 3421 | 17.716 | 17.795 | 0.45 |
| | 297.00 | 3349 | 17.717 | 17.876 | 0.90 |
| ρ_3 | 317.48 | 3308 | 17.722 | 18.474 | 4.24 |
| | 322.61 | 3032 | 17.729 | 18.727 | 5.63 |
| Square Tube ($L = 150$ mm, $t = 1.1$ mm, $c = 38.0$ mm) | | | | | |
| ρ_1 | 172.69 | 2516 | 10.518 | 9.485 | 9.82 |
| | 175.81 | 2456 | 10.560 | 8.101 | 23.29 |
| ρ_2 | 272.04 | 2366 | 10.646 | 11.912 | 11.89 |
| | 331.86 | 2812 | 10.652 | 11.879 | 11.52 |
| ρ_3 | 350.07 | 2352 | 10.713 | 14.355 | 34.00 |
| | 377.11 | 2413 | 10.728 | 14.644 | 36.50 |
| Square Tube ($L = 150$ mm, $t = 1.1$ mm, $c = 50.6$ mm) | | | | | |
| ρ_1 | 163.36 | 1954 | 14.270 | 11.865 | 16.85 |
| | 167.34 | 1974 | 14.274 | 11.971 | 16.13 |
| ρ_2 | 249.87 | 1934 | 14.430 | 12.387 | 14.16 |
| | 268.66 | 2059 | 14.434 | 12.520 | 13.26 |
| ρ_3 | 312.77 | 2217 | 14.472 | 16.375 | 13.15 |
| | 347.77 | 2243 | 14.522 | 16.847 | 16.01 |

Three different type of inserting saw dust methods during carrying out the experiment to determine the trend of mean load.

Result shows that as the saw dust density increases, the mean load would increase as well. The relative displacement between the dusts particles is closer at higher density. As long as they are compressed, dust particle exerts an increasing internal pressure against the tube wall, thus causes higher collapse load. Besides that, result also indicates that saw dust filled circular tube has the highest mean load as compare to the squares tube. The high mean load of circular tube is mainly caused by the wall thickness and also the amount of saw dust occupied per unit volume. As it is compressed by axial loading, the inner volume of tube becomes smaller and this would increase the saw dust density. Circular tube has a relatively smaller volume after compressed as compared to squares tube. Therefore a smaller inner volume would create a higher saw dust density, which leads to higher mean load.

For square tube ($L = 150 \text{ mm}$, $t = 1.1 \text{ mm}$, $c = 38.0 \text{ mm}$) and square tube ($L = 150 \text{ mm}$, $t = 1.1 \text{ mm}$, $c = 50.6 \text{ mm}$), saw dust greatly affects the mean load in axial compression experiment. As the saw dust density increases, the collapse load would be higher which causes mean load also increases. However, saw dust filled square tube ($L = 150 \text{ mm}$, $t = 1.1 \text{ mm}$, $c = 50.6 \text{ mm}$) has higher mean load than the square tube ($L = 150 \text{ mm}$, $t = 1.1 \text{ mm}$, $c = 38.0 \text{ mm}$). The higher mean load is due to the greater total amount of saw dust which can absorb more energy within the tube. Since square tube ($L = 150 \text{ mm}$, $t = 1.1 \text{ mm}$, $c = 50.6 \text{ mm}$) can insert more amount of saw dust than square tube ($L = 150 \text{ mm}$, $t = 1.1 \text{ mm}$, $c = 38.0 \text{ mm}$), therefore the energy absorbed by the saw dust would be higher, which also increases the mean load.

4.5.4 Comparison of plastic wavelength

On the contrary, plastic wavelength measures the size of inward and outward fold of tube specimens in axial compression loading. Table 4.7 shows the theoretical and experimental result of plastic wavelength for hollow tube.

Table 4.7: Theoretical and experimental plastic wavelength of hollow tube

| Specimen tube | 2H _{exp} (mm) | | | | 2H _m (mm) | Percentage difference |
|---|------------------------|-------|-------|---------|----------------------|-----------------------|
| | 1 | 2 | 3 | Average | | |
| Circular (L=100 mm, t=1.5 mm, D=25.3 mm) Trial 1 | 12.85 | 15.97 | 12.31 | 14.02 | 11.70 | 19.83 |
| Circular (L=100 mm, t=1.5 mm, D= 25.3 mm) Trial 2 | 14.55 | 13.64 | 14.82 | | | |
| Square (L=150 mm, t=1.1 mm, c=38 mm) Trial 1 | 26.05 | 32.12 | 35.93 | 30.65 | 22.94 | 33.61 |
| Square (L=150 mm, t=1.1 mm, c=38 mm) Trial 2 | 26.72 | 30.93 | 32.15 | | | |
| Square (L=150 mm, t=1.1 mm, c=50.6 mm) Trial 1 | 34.75 | 32.38 | 34.83 | 33.56 | 27.76 | 20.89 |
| Square (L=150 mm, t=1.1 mm, c=50.6 mm) Trial 2 | 33.41 | 36.53 | 29.46 | | | |

Results shows that hollow circular tube (L = 100 mm, t = 1.5 mm, D = 25.3 mm) has the lowest plastic wavelength with average 14.02 mm obtained from average experiment result. However, square tube (L = 150 mm, t = 1.1 mm, c = 50.6 mm) has higher plastic wavelength with average 33.56 mm as compared to square tube (L = 150 mm, t = 1.1 mm, c = 38.0 mm) with 30.65 mm. The plastic wavelength, folding length of tube is mainly caused by the side dimension (diameter for circular tube and side length for square tube) and the thickness, which can be seen from theoretical equation for circular tube is $0.95\sqrt{Dt}$ and square tube is $0.983\sqrt[3]{c^2t}$. The larger the side dimension and greater the thickness, the greater the plastic wavelength. As calculated from theoretical equation, the plastic wavelength for circular tube (L = 100 mm, t = 1.5 mm, D = 25.3 mm) is 11.70 mm whereas square tube (L = 150 mm, t = 1.1 mm, c = 38.0 mm) and square tube (L = 150 mm, t = 1.1 mm, c = 50.6 mm)

are 22.94 mm and 27.76 mm respectively. The comparison by percentage difference between the theoretical and experimental plastic wavelength is greater for square tube ($L = 150$ mm, $t = 1.1$ mm, $c = 38.0$ mm), which is 33.61 %, followed by square tube ($L = 150$ mm, $t = 1.1$ mm, $c = 50.6$ mm) with 20.89 % and then circular tube ($L = 100$ mm, $t = 1.5$ mm, $D = 25.3$ mm) at 19.83 %. The greater of percentage difference is caused by the sensitivity of scale measurement. The plastic wavelength is measured in millimetre, which is very small scale displacement. A small scale displacement will make the measurement to deviate from the theoretical value, thus causes higher percentage difference.



4.6 Load displacement characteristic

In the axial compression experiment, load displacement curve was plotted by the INSTRON Bluehill system to obtain the result. Appendix E shows one of the selected axial compression experimental results.

Circular tubes formed multi lobe mode while square tubes formed diamond mode which consisted of inward and outward folding. In load displacement curve, load initially increased proportional against the displacement, from which tubes deformed elastically. As the tube continued with progressive loading, it reaches yield strength, where the slope of the curve became less steeper, indicated that tube begins to form plastic deformation at certain location.

Figure 4.10 shows the load displacement curve of axial crushing circular tube ($L=100$ mm, $t=1.50$ mm, $D=25.3$ mm).

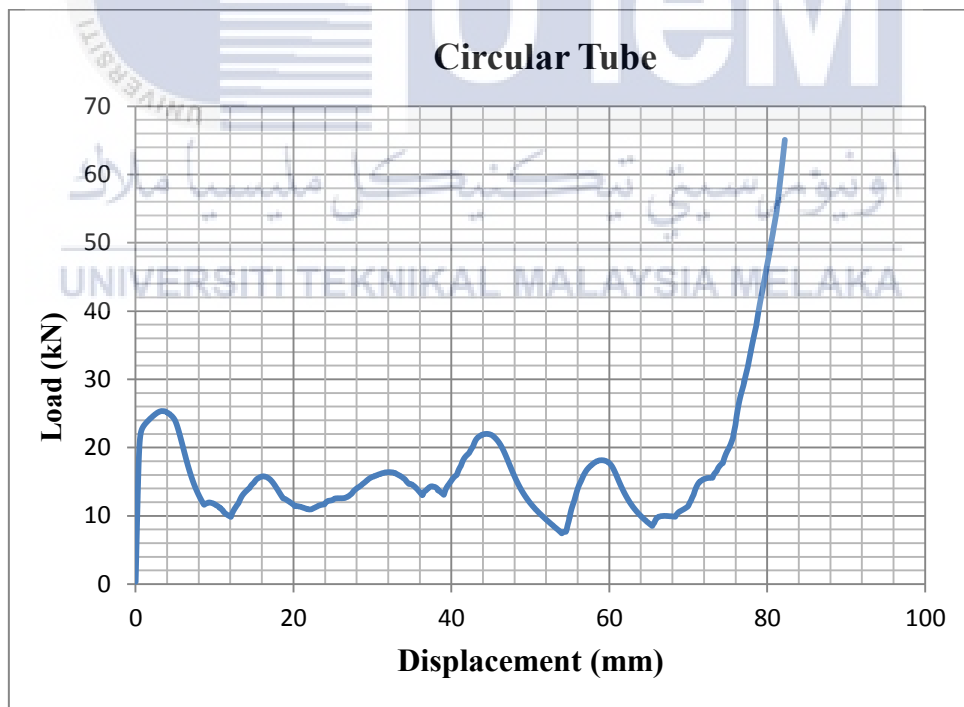
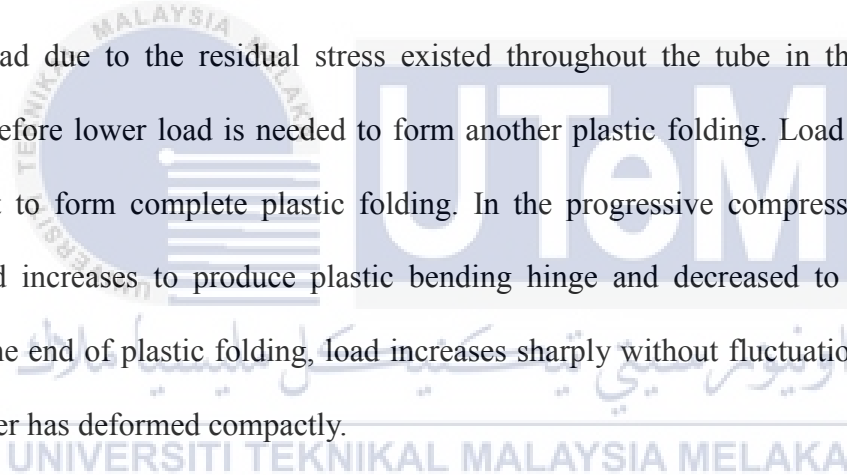


Figure 4.10: Load displacement curve of axial crushing circular tube ($L=100$ mm, $t=1.50$ mm, $D=25.3$ mm)

Load initially increased proportional against the displacement, indicates that circular tube deformed elastically. Hollow circular tube undergoes elastic behaviour from the origin until 21 kN at compressive displacement 0.5 mm. After 0.5 mm displacement, circular tube started to yield, from which load raised decreasingly to the peak load at 25 kN which is the first peak load where plastic bending line is produced. As the bending line formed, load decreased with displacement where tube deformed outward circumferentially at the end of the tube, from which the inner tube folds develop until they meet to each other. As the inner tube circumferential folds contact to each other, load increased to initiate another plastic bending line until 16 kN at 16 mm compressive displacement. The second peak load was lower to the first peak load due to the residual stress existed throughout the tube in the beginning of loading, therefore lower load is needed to form another plastic folding. Load decreased with displacement to form complete plastic folding. In the progressive compression quasi-static loading, load increases to produce plastic bending hinge and decreased to form complete folding. In the end of plastic folding, load increases sharply without fluctuation indicates that tube fold layer has deformed compactly.



As for hollow square tube ($L= 100$ mm, $t = 1.10$ mm, $c = 38.0$ mm), one of the load displacement curve has been obtained from the experiment work as shown in the Figure 4.11.

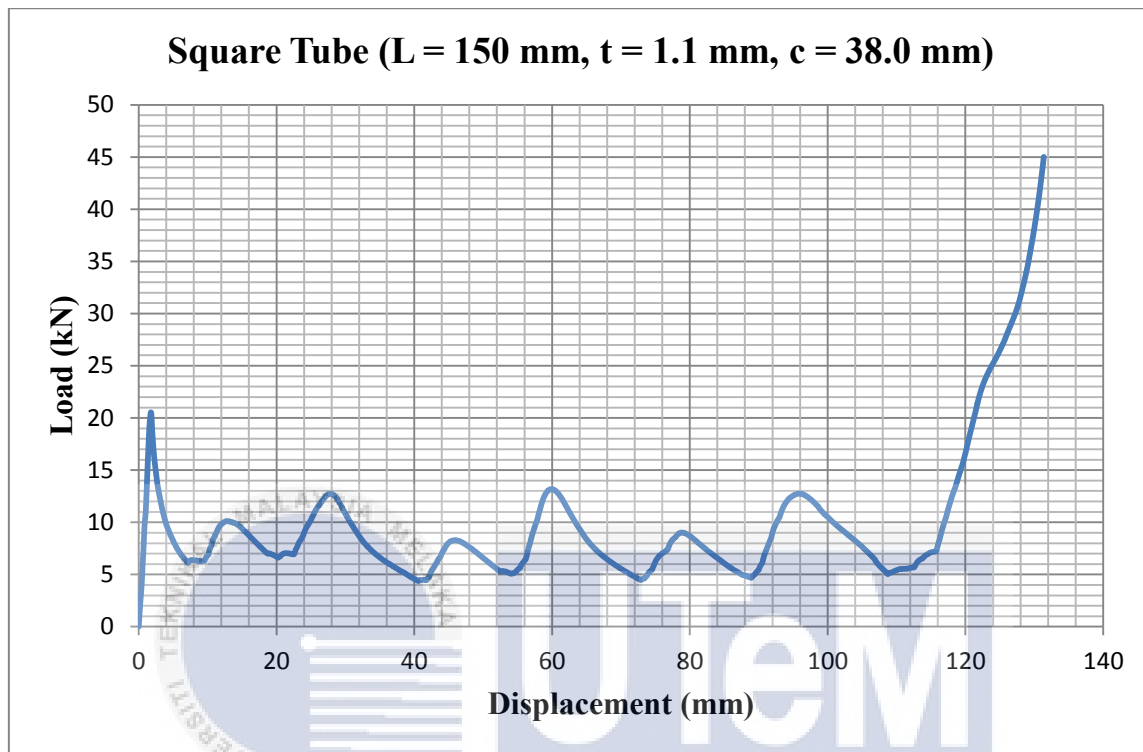


Figure 4.11: Load displacement curve of axial crushing square tube ($L= 100$ mm, $t = 1.10$ mm, $c = 38.0$ mm)

In the load displacement curve, hollow square tube undergoes elastic behaviour until 20.5 kN, which is the first peak load to initiate the bending line for folding. Load then decreased to about 6 kN and during the interval half fold is produced. Load increased again to 10 kN and then decreased to 7 kN at 23 mm compressive displacement to complete the plastic fold. Load increased to 13 kN at 28 mm compressive displacement to initiate another bending line. As plastic bending line produced, load decreased to 4.5 kN at 42 mm and during the time half fold is produced. Load increased again to 8 kN and then decreased to 5 kN at 54 mm compressive displacement to complete the plastic fold. Every plastic fold formed is equal to two successive with high and low fluctuated curves. During the end of plastic folding, load

increases sharply without fluctuation indicates that tube does not form fold layer and the tube will deformed compactly.

For hollow square tube ($L= 100$ mm, $t = 1.10$ mm, $c = 50.6$ mm), one of the load displacement curve has been obtained from the experiment work as shown in the Figure 4.12.

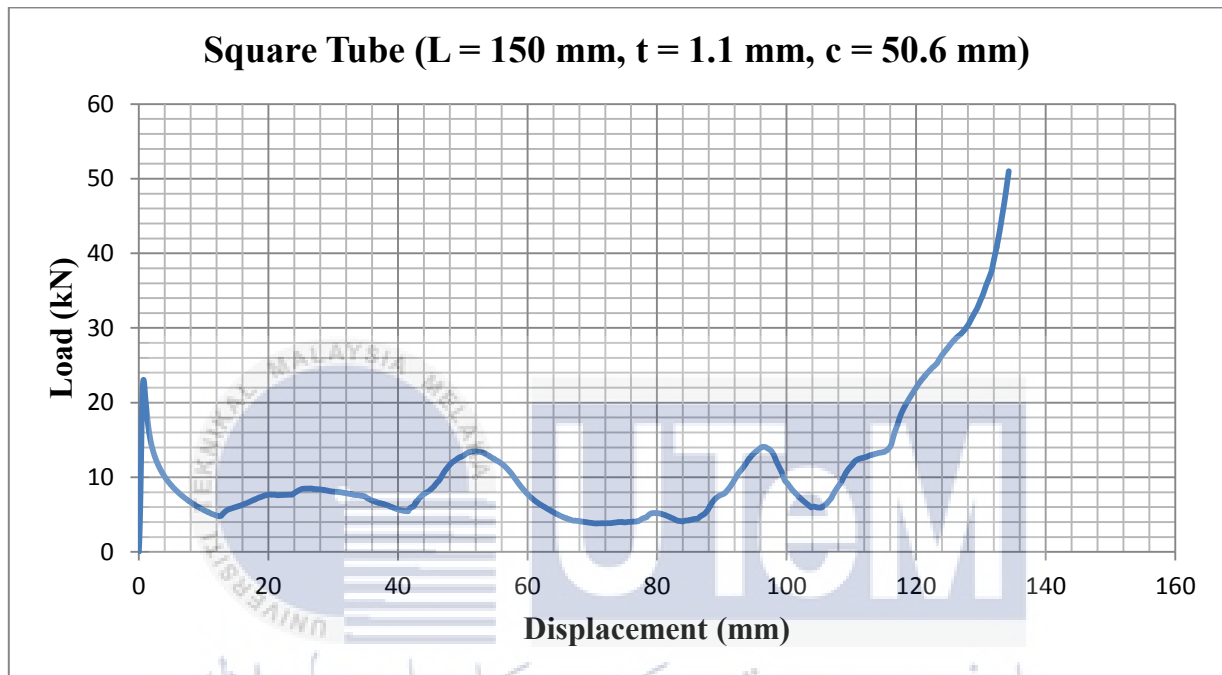


Figure 4.12: Load displacement curve of axial crushing square tube ($L= 150$ mm, $t = 1.10$ mm, $c = 50.6$ mm)

Load displacement curve shows that in the beginning of axial compression loading, load initially increased proportional against the displacement until 23 kN at compressive displacement of 1 mm, indicates that circular tube deformed elastically. At 1 mm compressive displacement, plastic bending line is produced. Load decreased to 5 kN at 12 mm compressive displacement to form half fold. Load increased again to 9 kN and then decreased to 5 kN at 42 mm compressive displacement to complete first fold. Load then increased to 13 kN at 52 mm compressive displacement to initiate another bending line. As plastic bending line produced, load decreased to 4 kN at 76 mm and during the time half fold is produced. Load then

increased slightly to 5 kN and then decreased back to 4 kN at 84 mm compressive displacement to complete the second fold. Each fold formed is equivalent to two successive high and low fluctuated curves. In the end of plastic folding, load increases sharply without fluctuation indicates that tube does not produce fold layer where tube crushed compactly.

However, as the tube inserted with saw dust at different density, different load displacement behavior produced. Figure 4.13 and Figure 4.14 shows the load displacement curve of axial crushing circular tube ($L= 100 \text{ mm}$, $t= 1.50 \text{ mm}$, $D = 25.3 \text{ mm}$) and square tube ($L= 100 \text{ mm}$, $t = 1.10 \text{ mm}$, $c = 38.0 \text{ mm}$) at different saw dust density respectively.

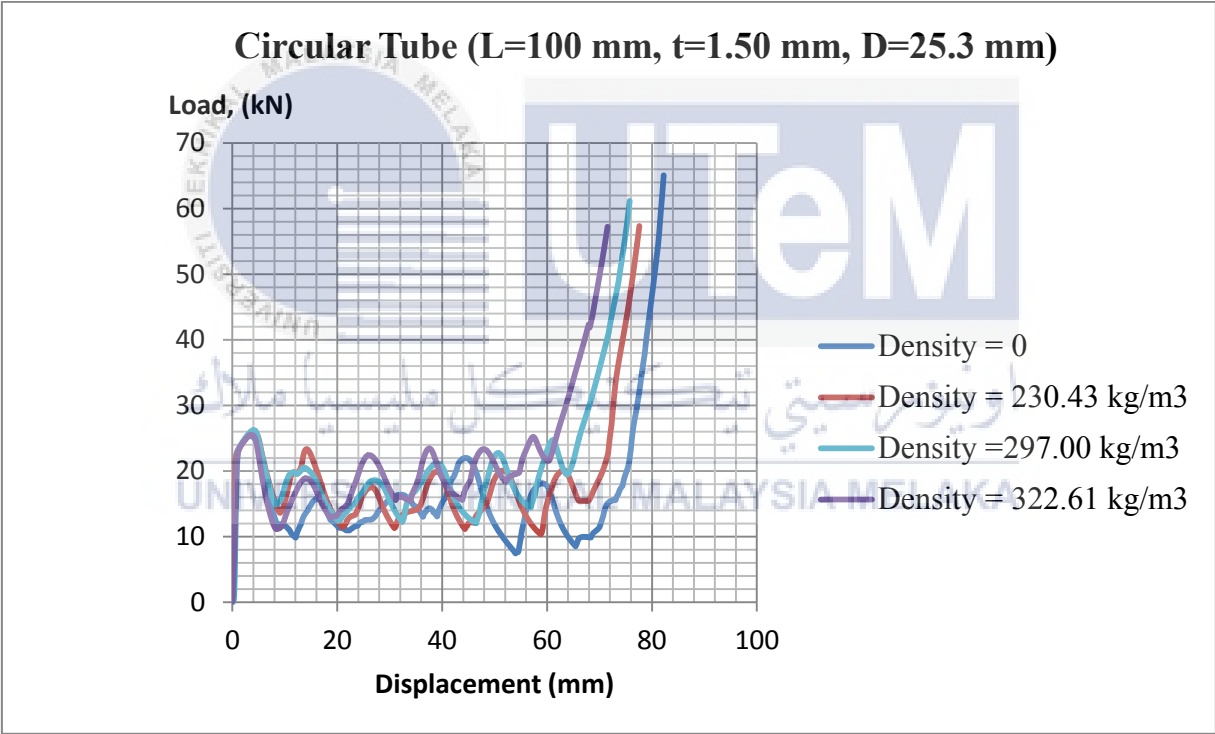


Figure 4.13: Load displacement curve of axial crushing circular tube ($L= 100 \text{ mm}$, $t= 1.50 \text{ mm}$, $D = 25.3 \text{ mm}$) at different density

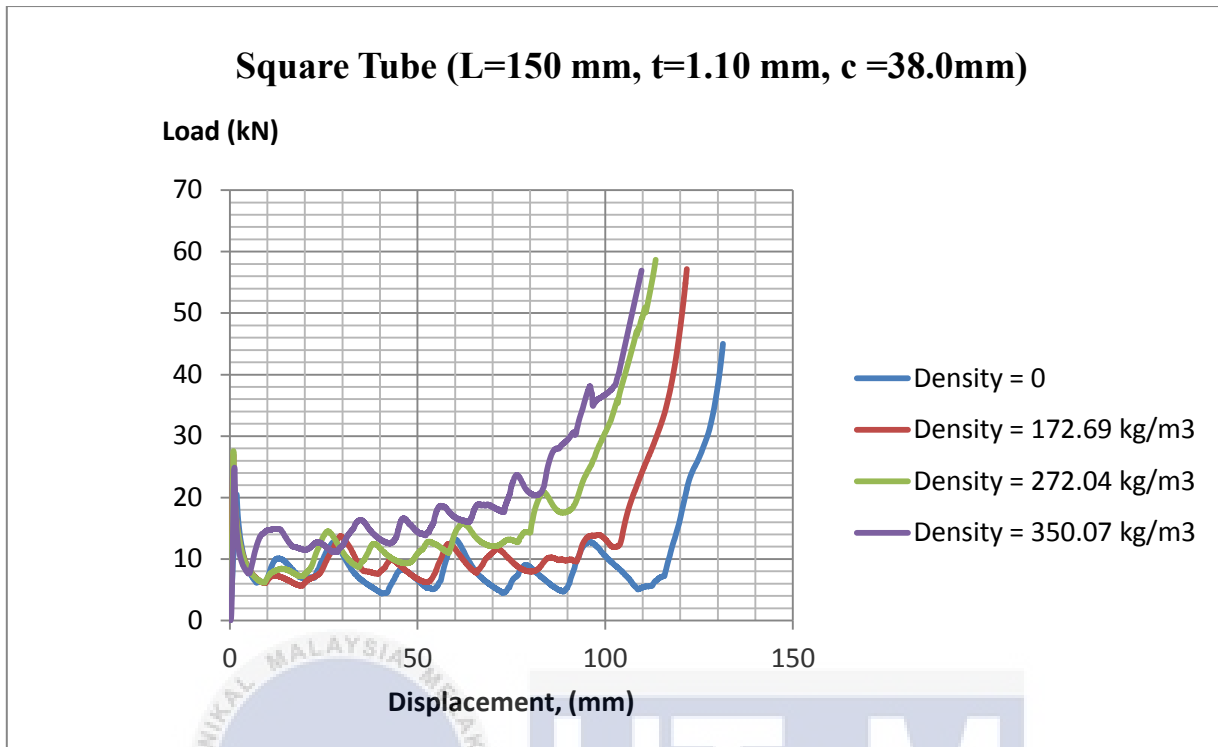


Figure 4.14: Load displacement curve of axial crushing square tube (L= 150 mm, t= 1.10 mm, c = 38.0 mm) at different density

Result shows that there is no relative difference in the first peak load at different density. This is because first peak load occurs at small compressive displacement, from which saw dust still consists available space to occupy. Therefore, the effect of saw dust does not affect the value of first peak load. The behaviour of load displacement curve of saw dust filled tube is characterised by initial high peak and then followed by upraise peak when the saw dust is densified. This subsequent of upraise peaks load are affected by increasing saw dust density. As the compressive displacement increases, the inner volume of tube decreases which would increase the saw dust density. Besides of increasing saw dust densified, saw dust has the friction interaction with the inner tube wall surface. This frictional interaction between the saw dust and the inner tube surface also contribute to the upraise peak load. Therefore, the resultant effect of saw dust density and the frictional interaction between saw dusts cause the increasing

of subsequent peak load at different density. Also, as the saw dust density increases, tube exhibits a decreasing in overall tube shortening. For a higher saw dust density, the amount of saw dust within the tube also higher as well. Therefore, a high density saw dust filled tube would achieve densification faster, where the load displacement curve does not fluctuate.

For saw dust filled square tube ($L= 150 \text{ mm}$, $t= 1.10 \text{ mm}$, $c= 50.6 \text{ mm}$), the experimental load displacement curve had not been determined as fully as expected. Figure 4.15 shows the load displacement curve of axial crushing square tube ($L= 150 \text{ mm}$, $t= 1.10 \text{ mm}$, $c = 50.6 \text{ mm}$) at different density.

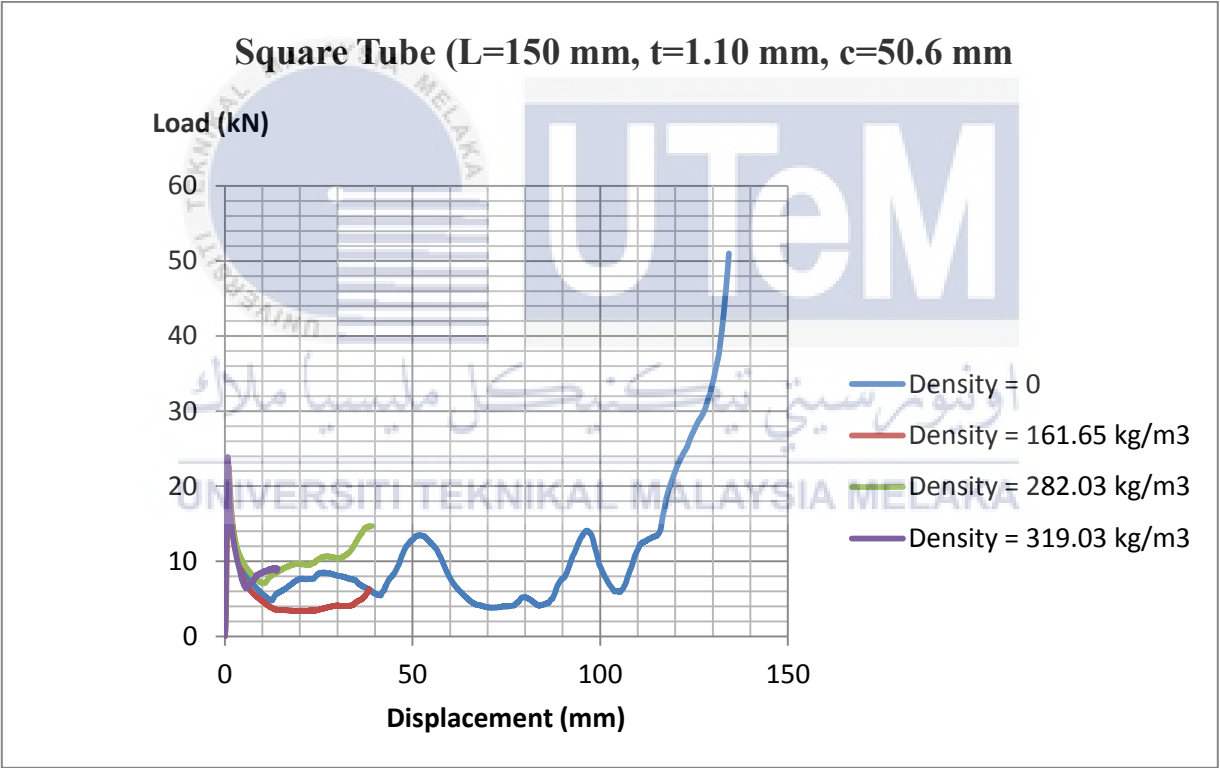


Figure 4.15: Load displacement curve of axial crushing square tube ($L= 150 \text{ mm}$, $t= 1.10 \text{ mm}$, $c = 50.6 \text{ mm}$) at different density

Result shows that only hollow tube shows successive folding as expected. However, saw dust filled square tube did not exhibit plastic folding but splitting during axial loading. Load displacement curve cannot be determined as tube splitting in axial compression loading. Figure 4.16 shows the photograph view of splitting square tube ($L= 150$ mm, $t= 1.10$ mm, $c = 50.6$ mm).

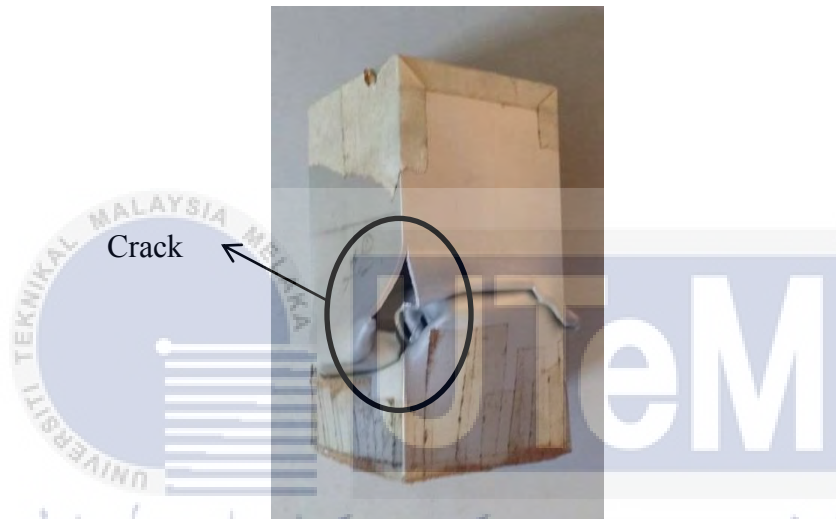


Figure 4.16: Photograph view of splitting square tube ($L= 150$ mm, $t= 1.10$ mm, $c = 50.6$ mm)

From Figure 4.16, saw dust filled square tube ($L= 150$ mm, $t= 1.10$ mm, $c = 50.6$ mm) frequently cracked at the corner of tube from a series experiment conducted. This is because during the axial compression loading, internal pressure is greater at the boundary area at the corner. Therefore saw dust can exert a big pressure toward the corner, which causes tube splitting.

4.7 Energy absorption

As the tube is upon on applied axial loading, work is done to crush the tube. Energy absorbed by the tube due to work done is dissipated into strain energy to produce deformation. Energy absorbed can be determined from the experimental work, which is the area under the load displacement curve. The amount of the energy absorbed depends on how much the load required to collapsing the tube.

By using saw dust as material to evaluate the performance, it shows that the energy absorption become greater. However, the specific energy absorbed becomes lower as the saw dust density increases. On the other hand, as the saw dust density increases, tube exhibits reduction of overall tube shortening (displacement at densification point decreases). Table 4.8, Table 4.9 and Table 4.10 show the displacement at densification point, energy absorbed and specific energy of using different type of specimens at different density.

Table 4.8: Densification point, energy absorbed and specific energy of circular tube (L= 100 mm, t= 1.50 mm, D = 25.3 mm) at different density

| Density (kg/m ³) | Total mass of tube and saw dust m _t + m _w (g) | Displacement at densification point (mm) | Energy absorbed (J) | Specific energy (kJ/kg) | |
|------------------------------|---|--|---------------------|-------------------------|--------|
| ρ ₀ | 0 | 29.8 | 81.0 | 1310 | 43.96 |
| | 0 | 29.9 | 82.5 | 1303 | 43.579 |
| ρ ₁ | 220.19 | 38.6 | 78.0 | 1374 | 35.596 |
| | 230.43 | 38.9 | 76.5 | 1380 | 35.476 |
| ρ ₂ | 297.00 | 41.5 | 74.25 | 1494 | 36.289 |
| | 297.00 | 41.5 | 74.5 | 1506 | 34.00 |
| ρ ₃ | 317.48 | 42.3 | 71.0 | 1535 | 36.288 |
| | 322.61 | 42.6 | 71.5 | 1557 | 36.549 |

Table 4.9: Densification point, energy absorbed and specific energy of square tube (L= 150 mm, t= 1.10 mm, D = 38.0 mm) at different density

| Density (kg/m ³) | | Total mass of tube and saw dust m _t + m _w (g) | Displacement at densification point (mm) | Energy absorbed (J) | Specific energy (kJ/kg) |
|------------------------------|--------|--|--|---------------------|-------------------------|
| ρ ₀ | 0 | 64.5 | 128.5 | 1189 | 18.434 |
| | 0 | 63.8 | 131.0 | 1283 | 20.110 |
| ρ ₁ | 172.69 | 94.6 | 120.0 | 1437 | 15.190 |
| | 175.81 | 96.6 | 120.0 | 1324 | 13.706 |
| ρ ₂ | 272.04 | 114.8 | 112.0 | 1813 | 15.793 |
| | 331.86 | 125.3 | 115.0 | 1908 | 15.227 |
| ρ ₃ | 350.07 | 130.7 | 103.0 | 1906 | 14.583 |
| | 377.11 | 135.3 | 105.0 | 2113 | 15.617 |

Table 4.10: Densification point, energy absorbed and specific energy of square tube (L= 150 mm, t= 1.10 mm, D = 50.6 mm) at different density

| Density (kg/m ³) | | Total mass of tube and saw dust m _t + m _w (g) | Displacement at densification point (mm) | Energy absorbed (J) | Specific energy (kJ/kg) |
|------------------------------|--------|--|--|---------------------|-------------------------|
| ρ ₀ | 0 | 79.3 | 132.5 | 1374 | 17.327 |
| | 0 | 78.6 | 133.0 | 1395 | 17.748 |
| ρ ₁ | 163.36 | 137.0 | - | - | - |
| | 167.34 | 138.4 | - | - | - |
| ρ ₂ | 249.87 | 167.2 | - | - | - |
| | 268.66 | 173.3 | - | - | - |
| ρ ₃ | 312.77 | 189.6 | - | - | - |
| | 347.77 | 201.6 | - | - | - |

Results show that as the saw dust density in the tube increases, the energy absorbed is increases, however the displacement at densification point is decreases. The higher energy absorbed is due to the total amount of saw dust within the tube. At densification point where the saw dust filled tube become inefficient in energy absorbed, the maximum displacement at densification point decreases due to the overall saw dust turns solidified earlier.

By comparing the three types of tube, circular tube has the highest specific energy compared to another both types of square tube. The higher specific energy of circular tube ($L=100$ mm, $t=1.50$ mm, $D=25.3$ mm) is because the total mass of tube is lower since the specific energy is equivalent to total energy absorbed per unit total tube mass. However by inserting the saw dust, the specific energy does not change much at increasing density. The reason is because as saw dust density increases, the total mass of tube and the energy absorbed increases. The increased of energy absorbed is compensated by the increased total mass of tube, showing no different in the specific energy. By comparing between the hollow tube and filled tube, hollow tube has higher specific energy due to it has smaller mass. For saw dust filled square tube ($L=150$ mm, $t=1.10$ mm, $D=50.6$ mm), the specific energy cannot be calculated due to the square tube splitting. The tube splitting causes the difficult of energy absorbed to be determined.

CHAPTER 5

CONCLUSION AND RECOMMENDATIONS

To conclude the topic of the study, it is important to understand the properties and deformation behavior of metallic tube before designing it into useful impact energy absorption devices. Therefore, it is necessary to review more studies and researches of the related resources. The related information of literature study about the topic has been introduced in this report. To design a potentially and useful impact energy absorption device, mode of deformation and load displacement curves should be used. The mean load, deformation fold length and energy absorption of the impact energy absorber (IEA) can be determined from load-displacement curve. Through the literature studies, crashworthiness of impact energy absorber is the main concern in order to further to design the impact energy devices.

From the experiment that had been conducted, it was shown that for circular tube ($L = 100$ mm, $t = 1.5$ mm, $D = 25.3$ mm), it deformed in multi lobe mode, square tube ($L = 150$ mm, $t = 1.1$ mm, $c = 38.0$ mm) and square tube ($L = 150$ mm, $t = 1.1$ mm, $c = 50.6$ mm) deformed in diamond mode. However, the deforming mode of circular and square tube does not affected by saw dust at different density. On the other hand, the presence of saw dust density would alter the mean load, energy absorbed and densification point where tube cannot longer to be compressed. The mean load was found that increases as the saw dust density increases. From the three different type of aluminium tube, circular tube ($L = 100$ mm, $t = 1.5$ mm, $D = 25.3$ mm) offers the highest mean load as compared to another two types square tube. Theoretical and experimental result also indicates that the plastic wavelength for circular

tube ($L = 100$ mm, $t = 1.5$ mm, $D = 25.3$ mm) has the lowest value as compared to another two type of square tube, indicates that the crushing behavior is most effective.

From load displacement curve, densification point, energy absorption and the specific energy can be determined. It was found that saw dust has the effect in the energy absorption characteristics. A higher energy absorber is more preferable to be as passive safety device to dissipate all kinetic energy of impact. Since saw dust density filled square tube ($L = 150$ mm, $t = 1.1$ mm, $c = 38.0$ mm) has the highest energy absorption analyzed from the experiment, therefore it is suitable to be used in passive safety energy absorber. However at higher density, crushing behavior becomes ineffective. To evaluate the superior impact energy absorption device, the specific energy has to be used. A higher specific energy of absorber would be more suitable to be as IEA device in the moving event. As compare between the three different types of aluminium tube, hollow circular tube ($L = 100$ mm, $t = 1.5$ mm, $D = 25.3$ mm) has the highest specific energy. Therefore, hollow circular tube was chosen as the best impact energy absorber in this topic study.

From experiment work that had been conducted, since the displacement at densification point, energy absorption and the specific energy of square tube ($L = 150$ mm, $t = 1.1$ mm, $c = 50.6$ mm) cannot be evaluated caused by tube splitting effect. Therefore it is recommended that a continuing experimental work is required so as to identify whether the square tube is good impact energy absorber or not. Besides using circular and square tube to perform axial loading compression experiment, it is suggested different shape type metal tube is used in this axial compression experiment such as triangular, rectangular or hexagonal tube. Therefore in the future, the impact energy absorbers would be improved in order to make the devices become more useful and more developed in application.

REFERENCES

- Andrews, K.R.F., England, G.L., & Ghani, E. (1983). Classification of the axial collapse of cylindrical tubes under quasi-static loading. *International Journal Mechanical of Science*, 25, pp. 687-696.
- Bachir, C., & Halima C. (2012). Effect of Adding Sawdust on Mechanical-Physical Properties of Ceramic Bricks to Obtain Lightweight Building Material. *International Journal of Mechanical, Aerospace, Industrial, Mechatronic and Manufacturing Engineering*, 2521-2525.
- Bardi, F.C. & Kyriakides, S. (2006). Plastic buckling of circular tubes under axial compression-part I: Experiments. *International Journal of Mechanical Sciences*, 48, 830-841.
- Emin Erdin, Cengiz, B., & Merve, T.C. (2016). Quasi-static axial crushing behaviour of thin-walled circular aluminium tubes with functionally graded thickness. *Procedia Engineering*, 559-565.
- Gan, N.F., Feng, Y.N., Yin, H.F., Wen, G.L., Wang, D.H., & Huang, X.Y. (2016). Quasi-static axial crushing experiment study of foam-filled CFRP and aluminium alloy thin-walled structures. *Composite Structures*, 303-319.

Guillow, S.R., Lu, G., & Grzebieta, R.H. (2001). Quasi-static axial compression of thin-walled circular aluminium tubes. *International Journal of Mechanical Sciences* , 2103-2123.

Gupta, N.K. (1998). Some aspects of axial collapse of cylindrical thin-walled tubes. *Thin-Walled Structures*, 32, 111-126.

Isabel, D., Lovre, K.O., & Matej, V. (2015). Characterisation of aluminium alloy tubes filled with aluminium alloy integral-skin foam under axial compressive loads. *Composite Structures*, 154-162.

Liu, Z.F., Hao, W.Q., Xie, J.M., Lu, J.S., Huang, R., & Wang, Z.H. (2015). Axial-impact buckling modes and energy absorption properties of thin-walled corrugated tubes with sinusoidal patterns. *Thin-Walled Structures*, 410-423.

Hossain, M.F., Islam, M.K., & Islam, M.A. (2014). Effect of chemical treatment on the mechanical and physical properties of wood saw dust particles reinforced polymer matrix composites. *Procedia Engineering*, 39-45.

Mateusz, S., Marek, M., Maciej, B., & Ewa, G. (2015). Mechanical properties of sawdust and woodchips. *Fuel*, 900-908.

Rafea, D.H., Dong, R., Lu, G.X., & Igor, S. (2016). Axial crushing behaviour of honeycomb-filled square carbon fibre reinforced plastic (CFRP) tubes. *Composite Structures*, 166-179.

Richard & Keith, J.N.G.B., (2015). *Shigley's Mechanical Engineering Design*. New York: McGraw-Hill Education.

Rizki, M., Tamai, Y., Takashi, Y., & Terazawa, M. (2010). Scrutiny on physical properties of sawdust from tropical commercial wood species: effects of different mills and sawdust's particle size. *Journal of Forestry Research*, 7, pp. 20-32.

S.R. Guillow., Lu, & R.H. Grzebieta, G. (2001). Quasi-static axial compression of thin-walled circular aluminium tubes. *International Journal of Mechanical Sciences*, 43, pp. 2103-2123.

Seitzberger, M., Rammerstorfer, F.G., Grading, R., Degischer, H.P., Blaimschein, M., & Walch, C. (2000). Experimental studies on the quasi-static axial crushing of steel column filled with aluminium foam. *International Journal of Solids and Structures*, pp. 4125-4147.

Singace, A.A. (1999). Axial crushing analysis of tubes deforming in the multi-lobe mode. *International Journal of Mechanical Sciences*, 865-890.

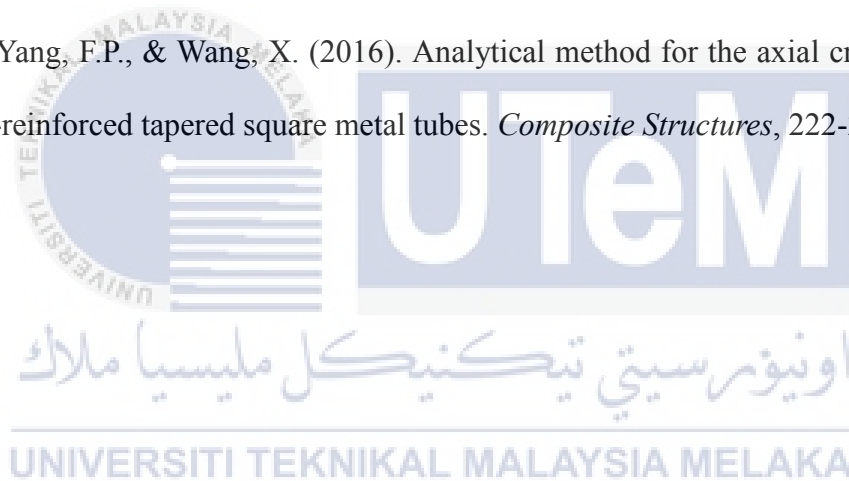
Singace, A.A. (2000). Collapse behaviour of plastic tubes filled with wood sawdust. *Thin-Walled Structures*, 37, pp. 163-187.

Takian, F., Rubayyat, M., & Islam, M.A. (2013). Properties of Wood Sawdust and Wheat Flour Reinforced Polypropylene Composites. *Journal of Modern Science and Technology*, 135-148.

Timothy A.P. (2014). *Mechanics Of Materials*. Hoboken: John Wiley & Sons, Inc.

Tohid, G.G., Hui, J., & Damien, H. (2015). Plastic buckling of dented steel circular tubes under axial compression: An experimental study. *Thin-Walled Structures*, 48-54.

Ying, L.W., Yang, F.P., & Wang, X. (2016). Analytical method for the axial crushing force of fiber-reinforced tapered square metal tubes. *Composite Structures*, 222-233.



APPENDIX A1: Gantt chart of PSM 1

Final Year Project 1

| Activity | Week | | | | | | | | | | | | | | |
|---|------|---|---|---|---|---|---|---|---|----|----|----|----|----|----|
| | 1 | 2 | 3 | 4 | 5 | 6 | 7 | 8 | 9 | 10 | 11 | 12 | 13 | 14 | 15 |
| Project Briefing and Planning | ■ | | | | | | | | | | | | | | |
| Literature Review and Collecting Information | | ■ | ■ | ■ | ■ | ■ | ■ | ■ | ■ | ■ | ■ | ■ | ■ | ■ | ■ |
| Preparation Progress Report | | | | ■ | ■ | ■ | ■ | | | | | | | | |
| Specimen Preparation | | | | | ■ | ■ | | | | | | | | | |
| Tensile Test Briefing | | | | | | ■ | | | | | | | | | |
| Perform Tensile Testing | | | | | | | ■ | | | | | | | | |
| Submission Progress Report | | | | | | | ■ | | | | | | | | |
| Preparation Presentation and Draft Final Report | | | | | | | | ■ | ■ | ■ | ■ | ■ | ■ | ■ | |
| Submission Draft Final Report | | | | | | | | | | | | | | | ■ |
| Seminar Presentation Final Year Project I | | | | | | | | | | | | | | | ■ |



APPENDIX A2: Gantt chart of PSM 2

Final Year Project 2

| Activity | Week | | | | | | | | | | | | | | |
|--|------|---|---|---|---|---|---|---|---|----|----|----|----|----|----|
| | 1 | 2 | 3 | 4 | 5 | 6 | 7 | 8 | 9 | 10 | 11 | 12 | 13 | 14 | 15 |
| Project Briefing and Planning | ■ | | | | | | | | | | | | | | |
| Literature Review and Collecting Information | ■ | ■ | ■ | ■ | ■ | ■ | ■ | ■ | ■ | ■ | ■ | ■ | ■ | | |
| Perform Preliminary Experiment Work | ■ | ■ | ■ | ■ | | | | | | | | | | | |
| Capturing Preliminary Experimental Result | | ■ | ■ | ■ | | | | | | | | | | | |
| Perform Repeating Experiment Work | | | ■ | ■ | ■ | | | | | | | | | | |
| Capturing Repeating Experimental Result | | | | ■ | ■ | | | | | | | | | | |
| Preparation Final Report Chapter 1: Introduction Chapter 2: Literature Review Chapter 3: Methodology Chapter 4: Result and Discussion Chapter 5: Conclusion | | ■ | ■ | ■ | ■ | ■ | ■ | ■ | ■ | ■ | ■ | ■ | ■ | ■ | |
| Correction Final Report | | | | | | | | | | | | | ■ | ■ | |
| Submission Final Report | | | | | | | | | | | | | | ■ | |
| Seminar Presentation Final Year Project II | | | | | | | | | | | | | | | ■ |

APPENDIX B1: Progressive crushing of saw dust filled circular tube (L= 100 mm, t= 1.50 mm, d= 25.3 mm)

Saw dust density, $\rho_3 = 322.61 \text{ kg/m}^3$



s = 5 mm



s = 10 mm



s = 20 mm



s = 30 mm



s = 40 mm



s = 50 mm



s = 60 mm

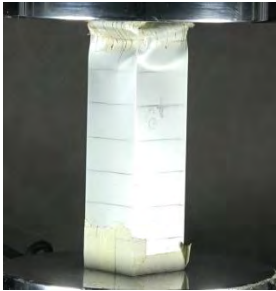


s = 70 mm

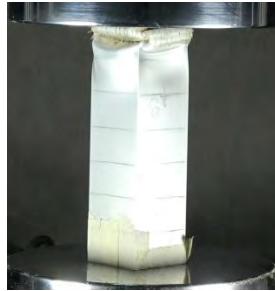
UNIVERSITI TEKNIKAL MALAYSIA MELAKA
UNIVERSITY OF TECHNOLOGY MALAYSIA MELAKA

APPENDIX B2: Progressive crushing of saw dust filled square tube (L=150 mm, t= 1.10 mm, c= 38.0 mm)

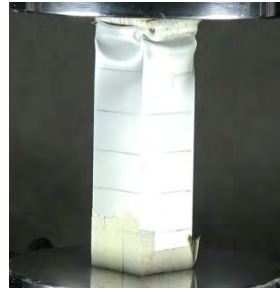
Saw dust density, $\rho_3 = 350.07 \text{ kg/m}^3$



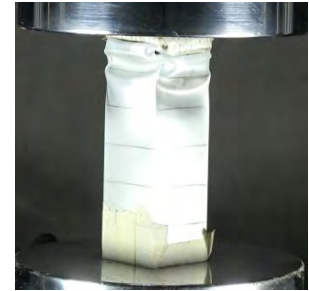
s = 10 mm



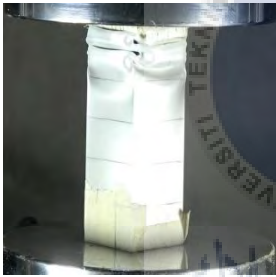
s = 20 mm



s = 30 mm



s = 40 mm



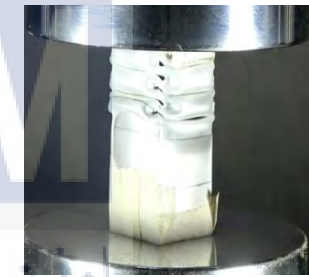
s = 50 mm



s = 60 mm



s = 70 mm



s = 80 mm



s = 90 mm



s = 100 mm

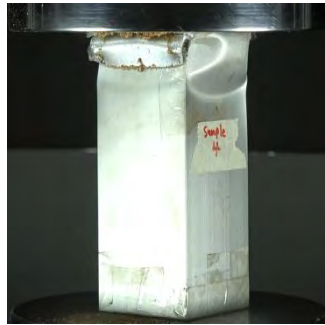
UNIVERSITI TEKNIKAL MALAYSIA MELAKA
UNIVERSITI TEKNIKAL MALAYSIA MELAKA
UNIVERSITI TEKNIKAL MALAYSIA MELAKA

APPENDIX B3: Progressive crushing of saw dust filled square tube (L=150 mm, t= 1.10 mm, c= 50.6 mm)

Saw dust density, $\rho_3 = 312.77 \text{ kg/m}^3$



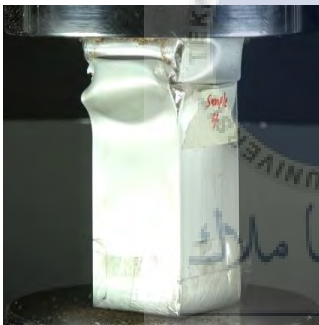
s = 10 mm



s = 20 mm



s = 30 mm



s = 40 mm



s = 50 mm



s = 60 mm

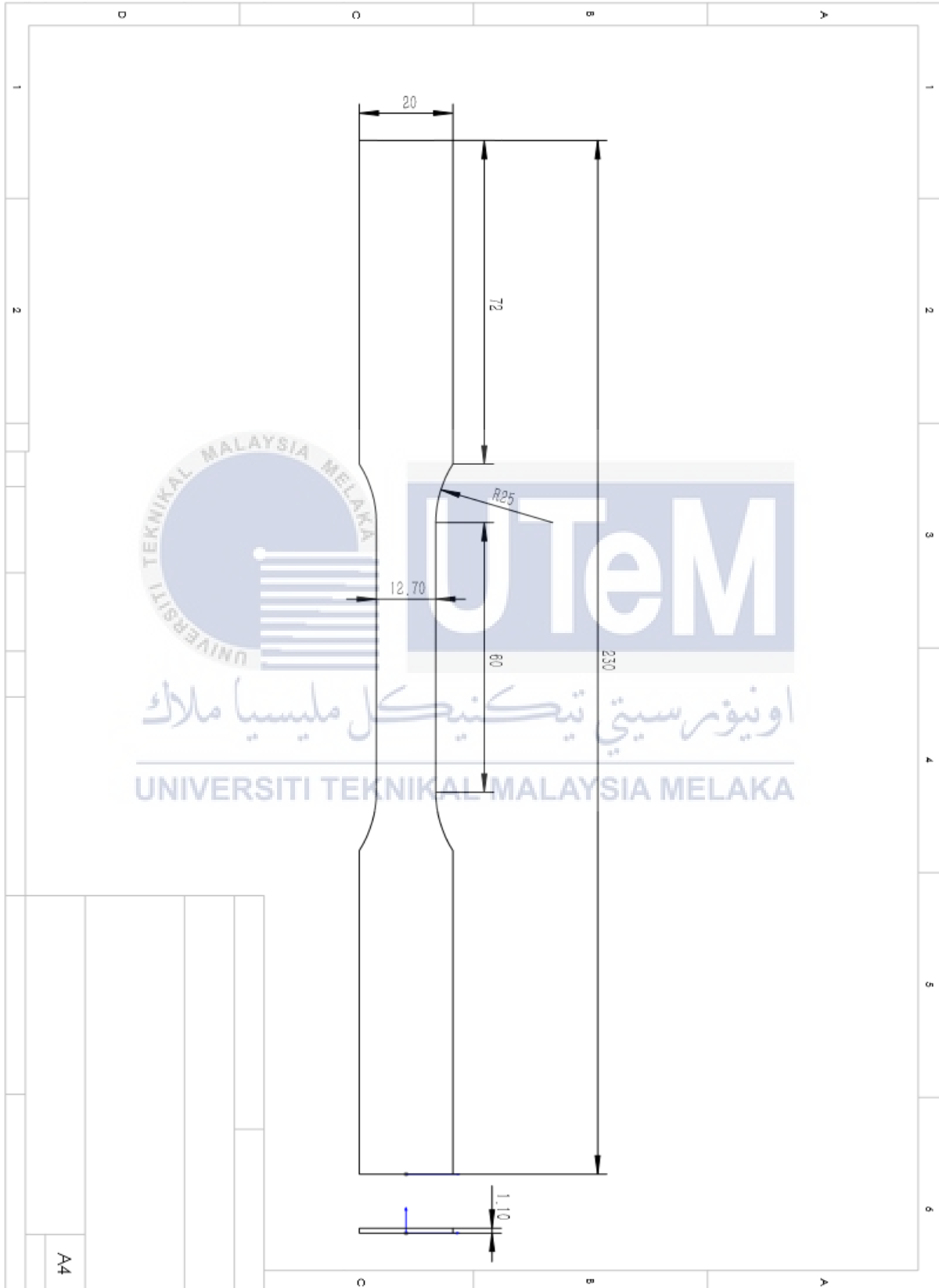


s = 70 mm



s = 80 mm

APPENDIX C: Tensile Test Specimen Dimension

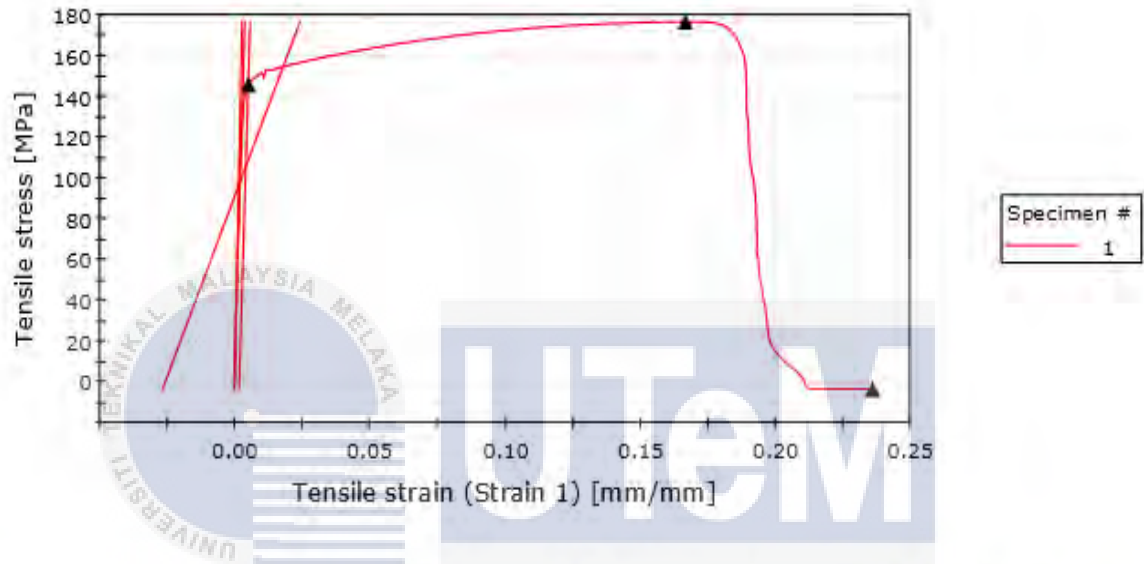


APPENDIX D: Tensile Test Specimen Result

Test: Rate 2

5.00000 mm/min

Aluminium Sample 1



| | Maximum Load [kN] | Tensile stress at Maximum Load [MPa] | Load at Yield (Offset 0.2 %) [kN] | Tensile stress at Yield (Offset 0.2 %) [MPa] |
|---|-------------------|--------------------------------------|-----------------------------------|--|
| 1 | 2.389 | 176.546 | 1.971 | 145.699 |

| | Load at Break (Standard) [kN] | Tensile stress at Break (Standard) [MPa] | Tensile extension at Break (Standard) [mm] |
|---|-------------------------------|--|--|
| 1 | -0.041 | -3.042 | 5.894 |

| | Tensile strain (Strain 1) at Break (Standard) [mm/mm] | Strain 1 at Break (Standard) [mm/mm] | Modulus (Automatic) [GPa] |
|---|---|--------------------------------------|---------------------------|
| 1 | 0.236 | 0.010 | 3.537 |

| | Modulus (Automatic Young's) [GPa] | Modulus (E-modulus) [GPa] |
|---|-----------------------------------|---------------------------|
| 1 | 67.270 | 43.960 |

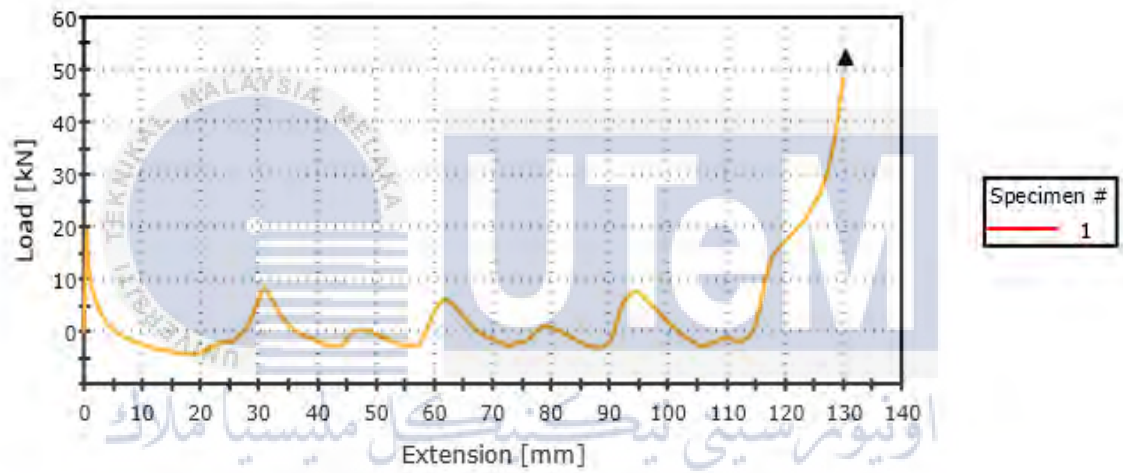
APPENDIX E: Axial Compression Experimental Result

Aluminium Square Tube

Aluminium Square Tube

| | |
|------------|-----------------------|
| nama bahan | Aluminium Square Tube |
|------------|-----------------------|

Aluminium Square Tube A1



UNIVERSITI TEKNIKAL MALAYSIA MELAKA

| | Max Load [kN] | Compressive stress at Maximum Load [MPa] | Compressive strain (Extension) at Maximum Load [mm/mm] | Compressive extension at Maximum Load [mm] |
|---|---------------|--|--|--|
| 1 | > 52.34657 | > 410.51 | > 5.21 | > 130.21 |

| | Area under curve [J] | Energy at Maximum Compressive stress [J] | Data point at Maximum Load |
|---|----------------------|--|----------------------------|
| 1 | 7.29 | 367.26 | 7839 |